J. Fluid Mech. (2011), *vol.* 666, *pp.* 521–553.
doi:10.1017/S0022112010004325

Overtopping a truncated planar beach

ANDREW J. HOGG[1]†, TOM E. BALDOCK[2] AND DAVID PRITCHARD[3]

[1]Centre for Environmental and Geophysical Flows, School of Mathematics, University of Bristol, University Walk, Bristol BS8 1TW, UK

[2]School of Civil Engineering, University of Queensland, Brisbane, QLD 4072, Australia

[3]Department of Mathematics and Statistics, University of Strathclyde, Livingstone Tower, 26 Richmond Street, Glasgow G1 1XH, UK

(Received 26 November 2009; revised 2 August 2010; accepted 11 August 2010; first published online 16 Novemeber 2010)

Run-up on a truncated impermeable beach is analysed theoretically and experimentally to find the volume of fluid, associated with a single wave event, that flows over the end of the beach. The theoretical calculations investigate the motion using the shallow-water equations and the fluid is allowed to flow freely over the end of the beach. Two models of wave events are considered: dam-break initial conditions, in which fluid collapses from rest to run-up and overtop the beach, and a waveform that models swash associated with the collapse of a long solitary bore. The calculations are made using quasi-analytical techniques, following the hodograph transformation of the governing equations. They yield predictions for the volume of fluid per unit width that overtops the beach, primarily as a function of the dimensionless length of the beach. These predictions are often far in excess of previous theoretical calculations. New experimental results are also reported in which the overtopping volumes due to flows initiated from dam-break conditions are studied for a range of reservoir lengths and heights and for a range of lengths and inclinations of the beach. Without the need for any empirically fitted parameters, good agreement is found between the experimental measurements and the theoretical predictions in regimes for which the effects of drag are negligible.

Key words: coastal engineering, hydraulic control, shallow water flows

1. Introduction

The run-up of waves on beaches and coastal structures is a topic both of fundamental interest in fluid dynamics and of practical importance: applications range from understanding the sediment transport which maintains or erodes beaches (e.g. Pritchard & Hogg 2005) to predicting the hazards posed by tsunami impact (Synolakis & Bernard 2006). A configuration which is of particular interest occurs when the sloping surface up which the waves run is truncated at some distance above the position of the undisturbed shoreline, as, for example, when waves impact a sharp-crested breakwater, a natural beach berm or when tsunamis overtop berms and dunes, with typical length scales of the truncated beaches in these examples ranging from tens to hundreds of metres. In this case, water is driven over the crest

† Email address for correspondence: a.j.hogg@bristol.ac.uk

of the beach and does not return in the backwash. This overtopping may represent a hazard to both people and infrastructure (Reis *et al.* 2008) and there is a pressing need for accurate predictive tools to assess the effectiveness of sea defences to wave overtopping during storms (Donnelly, Kraus & Larson 2006). Additionally, the water which overtops the beach may contaminate the region behind it, as when sea water invades a freshwater lagoon, possibly generating and sustaining a saline ecosystem (Donnelly *et al.* 2006). It may drive sediment over the crest and off the beach face (Kobayashi, Tega & Hancock 1996; Baldock *et al.* 2005), thus degrading the beach and rendering it more susceptible to storm damage. Overtopping and sediment overwash are also very important for the growth of beach berms, where sediment is deposited on the crest rather than transported offshore (Hine 1979; Weir, Hughes & Baldock 2006). Finally, the overtopping, by modifying the backwash, may significantly alter the morphodynamic effect of the wave (Hogg & Pritchard 2004*b*).

Modelling wave overtopping and the associated overwash of sediment has traditionally been tackled using empirical approaches, but more recently numerical models have been developed, which are based upon the integration of primitive governing equations for the fluid flow. (See Reis *et al.* 2008 and Donnelly *et al.* 2006 for reviews and comparisons of the various approaches.) In this study, we employ the nonlinear shallow-water equations to model the motion, following Hu, Mingham & Causon (2000) and Hubbard & Dodd (2002), amongst others, while noting that there will be situations in which there are appreciable vertical fluid accelerations and thus the motion falls outside of the dynamical regime modelled by these equations. However, as for many other coastal flows, the applicability of the shallow-water equations to wave run-up and overtopping is well established (Dodd 1998; Shiach *et al.* 2004; Brocchini & Dodd 2008) and we anticipate that they will model the motion accurately.

For some applications, it is important to consider overtopping under a long sequence of periodic or random waves (e.g. Dodd 1998; Shiach *et al.* 2004), but the simplest form of this problem occurs when a single wave breaks and runs up a beach. In the case when the beach is not truncated, there is an asymptotic description of the flow due to Shen & Meyer (1963), which takes the form of an analytical solution to the shallow-water equations. This was subsequently extended by Peregrine & Williams (2001) (hereafter PW01) to the case of a truncated beach, for which the dimensionless overtopping volume per unit width was calculated as a function of the dimensionless length of the beach.

Although most experimental work has considered sequences of waves, sufficient evidence exists to suggest that the PW01 model does not fully capture the process of single-wave overtopping. In particular, Baldock *et al.* (2005) carried out a series of experiments in which regular waves overtopped a truncated planar beach: they used an empirical correlation to relate the properties of these waves to the parameters in the model developed by Peregrine & Williams (2001), and compared their results for the maximum depth at the crest and for the variation of the overtopping volume with the length of the truncated beach. They demonstrated that the PW01 model substantially underestimated flow depths and thus overtopping rates, and that improved agreement could be found by using the semi-empirical model of Baldock & Holmes (1997) to describe the swash lens. These results motivated the development of a new numerical solution to the shallow-water equations (Guard & Baldock 2007), which was shown to predict flow depths better than the analytical expression proposed by Shen & Meyer (1963). This solution was later written in analytical form by Pritchard, Guard & Baldock (2008).

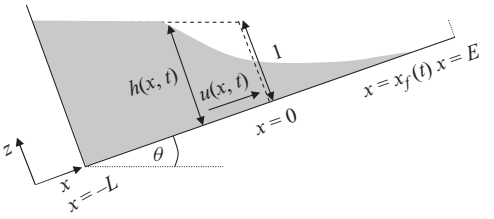

FIGURE 1. The configuration of the flow and the dimensionless variables that are used in the mathematical model. The dashed line shows the initial elevation of the fluid within the reservoir and that the dimensionless height of the confining dam is unity.

Another set of experiments which are relevant to this study was carried out by Baldock *et al.* (2007). They performed experiments on dam-break flow over a truncated planar beach (the same configuration as described below and depicted in figure 1). Fluid depths were compared successfully with the predictions from a numerical model, based on the shallow-water equations with friction (Baldock *et al.* 2007). The main focus of this study, however, was on sediment transport, and Baldock *et al.* (2007) did not present data for the volume of water overtopping the beach.

In this study, we calculate the volume of fluid per unit width that overtops a truncated planar beach, due to the run-up of a wave. The fluid motions are assumed to be sufficiently shallow so that they may be modelled by the nonlinear shallow-water equations and the incoming wave is generated by the instantaneous removal of a dam that confines elevated fluid (Antuono & Hogg 2009) or by offshore disturbances that generate waves of a specified form (Pritchard *et al.* 2008). Fluid may freely overtop the truncated beach while the conditions there are supercritical, but once critical conditions are established, there is a shoreward influence on the motion. Our results are obtained through quasi-analytical techniques, employing the hodograph transformation of the governing equations and building upon the methods recently developed by Hogg (2006), Pritchard *et al.* (2008), Antuono, Hogg & Brocchini (2009) and Antuono & Hogg (2009). These analytical methods offer several advantages over direct numerical integration of the governing equations in that they exploit the underlying characteristic structure of the dependent variables and provide considerable insight into the roles played by the initial and boundary conditions imposed on the flow. Typically the results are obtained through the solution of an integral equation, which is readily tackled using standard numerical techniques (see, for example, Hogg 2006 and § 3). For the overtopping flows analysed in this paper, we show that the PW01 model significantly underpredicts the volume of fluid that overtops the truncated beach, essentially because it is built upon a model of run-up that underpredicts the shoreward fluxes of fluid (Baldock *et al.* 2005). However, we show that their results are recovered when the length of the beach is close to, but just less than, the maximum run-up length of the wave, thus illustrating that the hydrodynamic solution of Shen & Meyer (1963), on which the PW01 model is built, is an asymptotic description of the motion close to the wavefront.

In this contribution, we also present the results of new laboratory experiments that investigate the volume of fluid that overtops a planar truncated beach. The fluid is released from a tilted flume from an initial state of rest behind a confining dam and flows along the inclined base, overflowing the end of the apparatus. When the fluid recedes and ceases overtopping, the end of the apparatus is then sealed and the volume collected is measured. We thus experimentally measure the overtopping associated

with only the first wave and not the subsequent reflections. This configuration corresponds precisely to that studied theoretically and thus we are able to confirm the theory by quantitatively comparing it with experimentally measured results. Indeed, we will show that the overtopping volume may be computed by specifying the values of two dimensionless parameters that specify the length of the reservoir and the length of the beach and that this produces results that are in close agreement with the experimental measurements without the inclusion of any empirically fitted parameters. Although the agreement is with inviscid theory, we do find that drag affects the motion by significantly curtailing the run-up along the inclined beach (Hughes 1995; Puleo & Holland 2001), thus preventing fluid overtopping when the end of the beach is sufficiently distant from the initially confining dam.

The paper is structured as follows. First we formulate the mathematical description of the flow and briefly introduce the hodograph transformation (§ 2). Overtopping due to dam-break flow is then calculated, first analysing the supercritical phase of the motion (§ 3.1) and then the motion with critical conditions imposed at the end of the truncated beach (§ 3.2). These yield predictions for the overtopping volumes of fluid per unit width (§ 3.3). We also analyse the effects of a bounded dam-break release of fluid by calculating the influence on the motion due to an impermeable back wall at the end of the reservoir that initially contains the fluid. We first calculate the hydrodynamics (see the Appendix) and then couple this description to the model of overtopping (§ 3.4). These calculations are quasi-analytical and exploit the hodograph transformation of the governing equations to form a single integral equation that is solved to determine the overtopping flux. Experiments that measure the overtopping volumes from dam-break releases in inclined flumes are reported in § 4 and the results are compared with the theoretical predictions in the same configuration. We then consider the overtopping volumes due to the waveform proposed by Guard & Baldock (2007) and compute them by following the same analytical techniques (§ 5). This calculation illustrates that the analytical framework developed here may be applied to other types of fluid motion. Finally we summarise our results and present some conclusions (§ 6).

2. Governing equations and the hodograph transformation

We analyse the two-dimensional motion of inviscid fluid along a planar beach on the assumption that the flow is predominantly parallel to the underlying boundary. This implies that fluid accelerations perpendicular to the plane are negligible and the pressure adopts a hydrostatic distribution. We first treat the motion that occurs when fluid is instantaneously released from a state of rest within a reservoir behind a dam, before calculating results for other waveforms (see § 5). This idealised initial condition captures many of the features of wave run-up on a beach: it exhibits a shoreline that runs up the beach before receding (its motion is essentially ballistic) and it leads to the formation of a backwash bore (Antuono & Hogg 2009). Furthermore, this initial condition is readily reproduced in experiments (see § 4).

We adopt x and z coordinate axes that are parallel and perpendicular to the plane, respectively, with the origin located at the base of the dam; the inclination of the plane is denoted by θ (see figure 1). Then the dimensionless shallow-water equations that govern the evolution of the depth of the flow, $h(x,t)$, and its velocity, $u(x,t)$, are given by (see Peregrine 1972)

$$\frac{\partial h}{\partial t}+\frac{\partial}{\partial x}(uh)=0 \quad \text{and} \quad \frac{\partial u}{\partial t}+u\frac{\partial u}{\partial x}+\frac{\partial h}{\partial x}=-1. \tag{2.1}$$

In these equations, length scales parallel and perpendicular to the plane have been rendered dimensionless with respect to $h_0^*/\tan\theta$ and h_0^*, respectively, where h_0^* denotes the initial dimensional height of fluid immediately behind the dam. Times are non-dimensionalised by $(h_0^*\cos\theta/g)^{1/2}/\sin\theta$, where g denotes gravitational acceleration. With these dimensional scales, we find that there are two dimensionless parameters remaining, $E \equiv \tan\theta E^*/h_0^*$ and $L \equiv \tan\theta L^*/h_0^*$, which essentially measure the length of the beach (E^*) and the length of the reservoir (L^*) relative to the length scale of the fluid flow.

The initial conditions are that $u(x,0)=0$ and

$$h(x,0) = \begin{cases} 1-x, & -L \leqslant x \leqslant 0, \\ 0, & x > 0. \end{cases} \tag{2.2}$$

The boundary conditions are that there is no flow at the back wall, $u(-L,t)=0$, and that a shoreline forms, $x_f(t)$, where the depth of the fluid vanishes, $h(x_f,t)=0$, until the end of the truncated beach at $x=E$ is reached at $t=t_s$. Thereafter while the motion is supercritical at $x=E$, the fluid flows off the end of the beach and out of the domain. Eventually, however, the Froude number ($F=u/\sqrt{h}$) at the end of the beach drops and the flow first becomes critical ($F=1$) at $t=t_*$. Then, following Peregrine & Williams (2001), we assume that the end of the beach acts as a hydraulic control point on the flow and we impose

$$u = \sqrt{h} \quad \text{at} \quad x = E, \quad \text{for} \quad t > t_*. \tag{2.3}$$

This way, we treat the end of the beach as a broad-crested weir, at which the flow undergoes the transition from a subcritical to a supercritical state. Alternatively, and this is closer to the experimental configuration, the end of the beach is a free overfall where the flow also passes from a sub- to a supercritical state. In this configuration, it is likely that critical conditions are attained slightly upstream of the overfall. However, the distance upstream is typically a few multiples of the flow depth, thus permitting the condition of criticality to be enforced at the end to a good approximation (Henderson 1966). Other configurations at the end of the beach are possible, such as a sharp-crested weir: these are typically associated with an empirical discharge expression that could be written in a form similar to (2.3), though possibly with a different constant of proportionality, thus allowing the general formulation that follows to be applied.

It is possible to maintain the boundary condition (2.3) until the depth of fluid at $x=E$ vanishes at $t=t_f$ and thereafter the shoreline retreats. If the reservoir is of infinite length, this sequence of flow events occurs provided $E>1$; for shorter beaches, $E<1$, the flow evolves to a steady state in which overtopping occurs indefinitely and thus there is no time, t_f, at which the flow begins to recede. In contrast, for finite-length reservoirs and for the waveforms of §4, there is always an upper bound to the volume of fluid overtopping the end of the truncated beach.

The shallow-layer model (2.1) neglects hydraulic resistance, an assumption that is most questionable when the flow depths are small so that the drag forces may significantly retard the motion. These resistive forces are particularly significant close to the front of the flow, where the depth vanishes and, analogously to dam-break flows over horizontal surfaces (Whitham 1955; Hogg & Pritchard 2004*a*), they may be no longer negligible, generating a drag-affected region close to the front. However, once the front has passed and the flow begun to overtop, the depth increases and the drag may become less significant until the overtopping phase nears its end and the flow depths become small again. In §4 where the experimental results are presented,

it is evident that for flows initiated from a dam-break configuration at laboratory scales, drag may significantly curtail the run-up (cf. Whitham 1955; Miller 1968; Hogg & Pritchard 2004*a*), but that accurate predictions of the overtopping volumes are obtained using an inviscid model of the motion. This is because the volume of fluid associated with the drag-affected tip is small relative to the remaining volume of overtopping fluid that follows it, unless the beach approaches the maximum length for overflow.

The governing equations (2.1) can be rewritten in characteristic form as follows:

$$\alpha \equiv u + t + 2c = \text{constant} \qquad \text{along curves such that} \qquad \dot{x} = u + c, \tag{2.4}$$

$$\beta \equiv u + t - 2c = \text{constant} \qquad \text{along curves such that} \qquad \dot{x} = u - c, \tag{2.5}$$

where $c = \sqrt{h}$ and where a dot denotes differentiation with respect to time. Using α and β as independent variables instead of x and t (the hodograph transformation), we find that $u = (\alpha + \beta)/2 - t$ and $c = (\alpha - \beta)/4$, while (2.4) and (2.5) become

$$\frac{\partial x}{\partial \beta} = \left(\frac{3\alpha + \beta}{4} - t\right)\frac{\partial t}{\partial \beta} \qquad \text{along curves such that} \qquad \alpha = \text{constant}, \tag{2.6}$$

$$\frac{\partial x}{\partial \alpha} = \left(\frac{\alpha + 3\beta}{4} - t\right)\frac{\partial t}{\partial \alpha} \qquad \text{along curves such that} \qquad \beta = \text{constant}. \tag{2.7}$$

Combining (2.6) and (2.7), we find that

$$\frac{\partial^2 t}{\partial \alpha \partial \beta} = \frac{3}{2(\alpha - \beta)}\left(\frac{\partial t}{\partial \alpha} - \frac{\partial t}{\partial \beta}\right). \tag{2.8}$$

The hodograph transformation remains invertible provided the Jacobian of the transformation, J, remains finite and non-vanishing. By using (2.6) and (2.7), it is possible to show that

$$J \equiv \frac{\partial t}{\partial \alpha}\frac{\partial x}{\partial \beta} - \frac{\partial t}{\partial \beta}\frac{\partial x}{\partial \alpha} = 2c\frac{\partial t}{\partial \alpha}\frac{\partial t}{\partial \beta}. \tag{2.9}$$

To solve this problem analytically, we use the scheme described in Hogg (2006), which employs a Green's function in the hodograph plane and utilises the linear differential form given by $\omega = -V\,\mathrm{d}a + U\,\mathrm{d}b$, in which

$$V = \frac{3tB}{2(a-b)} + \frac{B}{2}\frac{\partial t}{\partial a} - \frac{t}{2}\frac{\partial B}{\partial a} \quad \text{and} \quad U = -\frac{3tB}{2(a-b)} + \frac{B}{2}\frac{\partial t}{\partial b} - \frac{t}{2}\frac{\partial B}{\partial b}. \tag{2.10}$$

In these expressions, $B = B(a, b; \alpha, \beta)$ is the Riemann function that satisfies the partial differential equation adjoint to (2.8), which is given by

$$\frac{\partial^2 B}{\partial a \partial b} + \frac{3}{2(a-b)}\left(\frac{\partial B}{\partial a} - \frac{\partial B}{\partial b}\right) - \frac{3B}{(a-b)^2} = 0, \tag{2.11}$$

subject to the boundary conditions

$$\frac{\partial B}{\partial b} = \frac{-3B}{2(a-b)} \quad \text{along } a = \alpha, \quad \frac{\partial B}{\partial a} = \frac{3B}{2(a-b)} \quad \text{along } b = \beta \quad \text{and} \quad B(\alpha, \beta; \alpha, \beta) = 1. \tag{2.12}$$

In this case, the Riemann function is given by Garabedian (1986)

$$B(a, b; \alpha, \beta) = \frac{(a-b)^3}{(a-\beta)^{3/2}(\alpha - b)^{3/2}} F\left[\frac{3}{2}, \frac{3}{2}; 1; \frac{(a-\alpha)(\beta - b)}{(a-\beta)(\alpha - b)}\right], \tag{2.13}$$

where F is the hypergeometric function (Abramowitz & Stegun 1964). Accordingly, the solution $t(\alpha, \beta)$ satisfies (2.8) if the linear differential form ω is exact, that is, for all regular domains, D, in the (α, β) plane, we require that

$$\int_{\partial D} \omega = 0, \tag{2.14}$$

where ∂D represents the boundary of D.

3. Overtopping from dam-break flows

3.1. *Initial motion and supercritical overtopping*

From the dam-break initial conditions on a non-truncated beach (see (2.2)), Antuono & Hogg (2009) demonstrated that the motion, in terms of the hodograph variables, is given by

$$t = \int_2^\alpha B(a, -2; \alpha, \beta) \left[\frac{3}{4}\frac{(a-2)}{(a+2)} + \frac{1}{2}\right] \mathrm{d}a, \tag{3.1}$$

$$x = \left(\frac{\alpha + 3\beta}{4} - \frac{t}{2}\right) t - \frac{1}{4}\int_2^\alpha t(a, \beta)\, \mathrm{d}a. \tag{3.2}$$

This expression is valid within the expansion fan $-t^2/4 - t < x < x_f(t)$; fluid outside this fan remains at rest. The shoreline motion is a singular point within the hodograph plane with $\alpha = \beta = 2$. It is not possible to evaluate it from (3.1), but directly from the definition of the characteristic curves, it may be shown that the shoreline moves ballistically up the beach and is given by

$$x_f = 2t - t^2/2. \tag{3.3}$$

At this stage, we note that the solution for the flow derived by Shen & Meyer (1963), on which the PW01 model of overtopping is built, corresponds to (3.1) and (3.2) in the regime $\alpha - 2 \ll 1$. Thus, their solution corresponds to the region close to the shoreline. Shen & Meyer's solution may be considered as being generated from the collapse of fluid with a constant initial dimensionless depth of unity behind the dam, rather than the initial conditions treated here (cf. (2.2)). It is therefore anticipated that such a flow will lead to the forward propagation of a reduced volume of fluid compared to that initiated from (2.2) and thus the potential overtopping volumes are considerably reduced as well. This expectation will be established in the results that follow. However, when the beach is relatively long so that only fluid close to the shoreline may overtop ($2 - E \ll 1$), the asymptotic form of the flow field for $\alpha - 2 \ll 1$ will accurately represent the motion and our results for overtopping volumes in this regime converge to those of PW01.

From (3.3), it is straightforward to find the earliest time at which the flow reaches the end of the beach. This occurs at

$$t = t_s \equiv 2 - \sqrt{4 - 2E}. \tag{3.4}$$

For $t > t_s$, the fluid overtops the truncated beach. Initially there is supercritical flow at the end of the truncated beach, but as the flow slows and deepens, critical conditions are attained and thereafter the motion differs from that calculated by Antuono & Hogg (2009). The flow first becomes critical ($u = \sqrt{h}$) at the end of the beach when, in terms of hodograph variables, $t = (\alpha + 3\beta)/4$. Thus, denoting the onset of criticality

by $(t, \alpha, \beta) = (t_*, \alpha_*, \beta_*)$, we solve

$$t(\alpha_*, \beta_*) = \frac{\alpha_* + 3\beta_*}{4} \quad \text{and} \quad x(\alpha_*, \beta_*) = E. \tag{3.5}$$

The variation of these values with E is plotted in figure 2. We note that in the regime $\delta \equiv 2 - E \ll 1$,

$$t_* = 2 - \frac{\delta}{2} + \cdots, \quad \alpha_* = 2 + \frac{1}{2}\left(\frac{2}{3}\right)^{3/2}\delta^{3/2} + \cdots \quad \text{and} \quad \beta_* = 2 - \frac{2\delta}{3} + \cdots. \tag{3.6}$$

Furthermore, in the regime $0 < E \ll 1$, we find that

$$t_* = \frac{3\sqrt{6}}{8}\Delta + \cdots, \quad \alpha_* = 2 + \Delta + \cdots \quad \text{and} \quad \beta_* = -\frac{2}{3} + \frac{3\sqrt{6} - 2}{6}\Delta + \cdots, \tag{3.7}$$

where $\Delta = 8\sqrt{(9 + \sqrt{6})E}/15$.

In the Appendix, we show that the first α-characteristic that is affected by the impermeable back wall is given by $\alpha_{ws} = 4(1 + L)^{1/2} - 2$. Thus, the establishment of critical conditions at the end of the truncated beach is unaffected by the back wall if $\alpha_* < \alpha_{ws}$ and so we may determine a minimum length of reservoir, L_{crit}, such that the onset of critical conditions is unaffected by the reservoir length if $L > L_{crit}$. We plot the variation of L_{crit} with the length of the beach, E, in figure 2(b).

3.2. *Critical overtopping*

For $t > t_*$, the overflow at the end of the beach acts as a control on the fluid motion such that critical conditions ($u = \sqrt{h}$) are maintained at this location. As a consequence, the overflow at the end of the beach now affects the motion upstream and, in this subsection, we calculate the ensuing motion in terms of hodograph variables.

It is convenient to consider the modification to the motion in both the hodograph (α, β) and physical (x, t) planes (see figures 3 and 4). Offshore of the $\beta = \beta_*$ characteristic and onshore of the $\alpha = \alpha_*$ characteristic, the motion is unaffected by the overtopping at the end of the beach. The flow first becomes critical at the point $A = (\alpha_*, \beta_*)$ in the hodograph plane. The curve SA represents the variation of the hodograph variables at the end of the beach during the supercritical overtopping. The curve AB represents the hodograph variables at the end of the beach during the critical overtopping; it is written as $(\alpha, \beta_c(\alpha))$ and the determination of β_c remains one of the aims of this subsection. Provided the beach is sufficiently long ($E > 1$), this curve intersects $\beta = \alpha$ and then a receding shoreline forms and overtopping finishes after some finite time ($t = t_f$).

During the phase of the motion with critical conditions at $x = E$, we impose that $u = \sqrt{h}$, which implies that $t = (\alpha + 3\beta_c)/4$. Furthermore, treating $x \equiv x(\alpha, \beta)$, we find that at the end of the beach

$$\frac{\mathrm{d}x}{\mathrm{d}\alpha} = \frac{\partial x}{\partial \alpha} + \beta_c' \frac{\partial x}{\partial \beta} = \frac{\alpha - \beta}{2}\beta_c' \frac{\partial t}{\partial \beta} = 0, \tag{3.8}$$

where $\beta_c' \equiv \mathrm{d}\beta_c/\mathrm{d}\alpha$ and the final simplification comes from the equations along the characteristics (see (2.6), (2.7)). Using (3.8) we may also evaluate the derivative of t along the curve $\beta = \beta_c$: this is given by

$$\frac{\mathrm{d}t}{\mathrm{d}\alpha} = \frac{\partial t}{\partial \alpha} = \frac{1 + 3\beta_c'}{4}. \tag{3.9}$$

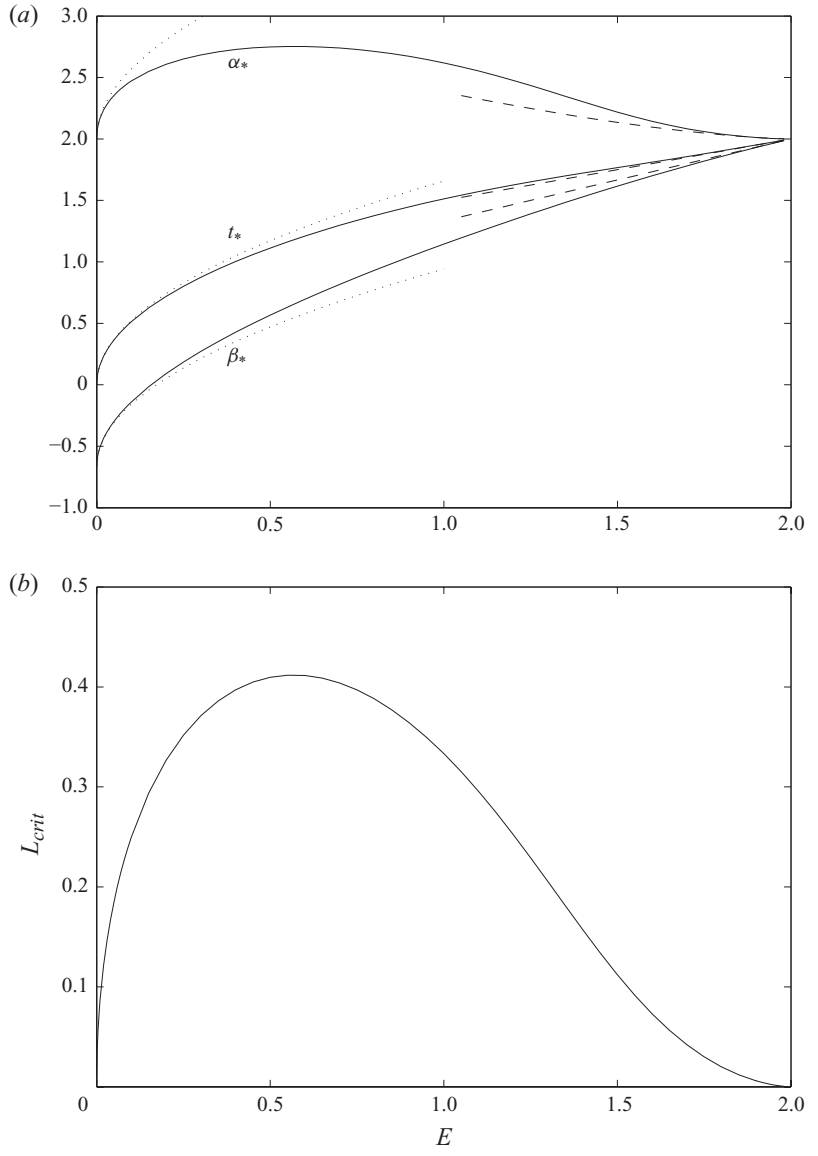

FIGURE 2. (*a*) The values of the characteristic variables, α_* and β_*, and the time, t_*, at which critical conditions are first attained at the end of the truncated beach as a function of the length of the beach, E. Also plotted are the asymptotic approximations for these quantities in the regimes $E \ll 1$ and $2-E \ll 1$. (*b*) The minimum length of reservoir, L_{crit}, such that if $L > L_{crit}$, critical conditions are attained at the end of the truncated beach before the dam-break flow is modified by the presence of the back wall.

In the hodograph plane, the region influenced by the critical overflow condition at $x = E$ is bounded by the curve AB and the characteristic $\beta = \beta_*$. Within this region, we employ Riemann's method to construct the solution. This is based upon integrating around the closed contour $ABCD$, where

$$A = (\alpha_*, \beta_*), \quad B = (\alpha, \beta_c(\alpha)), \quad C = (\overline{\alpha}, \beta_c(\alpha)) \quad \text{and} \quad D = (\overline{\alpha}, \beta_*). \tag{3.10}$$

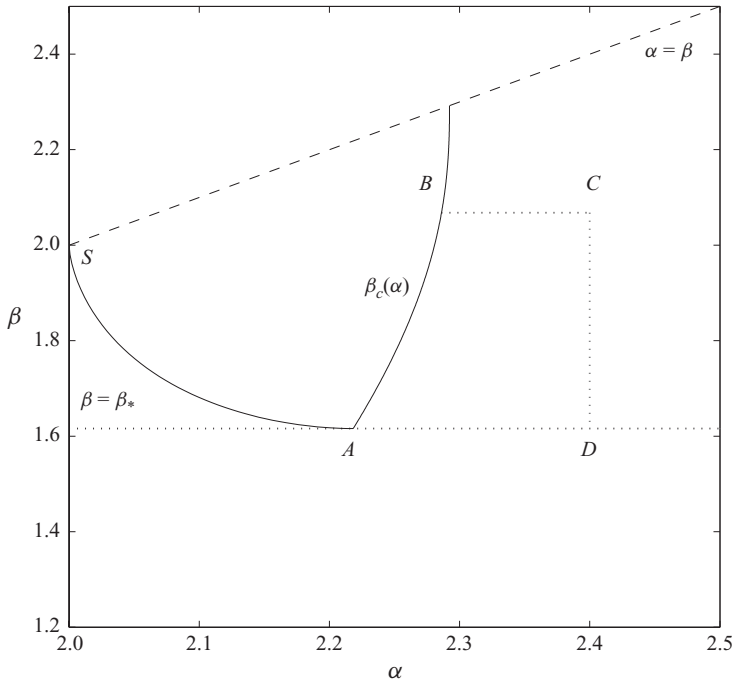

FIGURE 3. The hodograph plane for $E = 1.5$. Supercritical overtopping occurs at $x = E$ along the curve SA and critical overtopping at $x = E$ along the curve $\beta_c(\alpha)$. The closed contour $ABCD$ is used to construct the solution in the regions influenced by the critical overtopping. The depth of the flowing layer vanishes along the dashed line ($\alpha = \beta$).

The contribution from the segment BC is given by

$$\int_{\alpha}^{\overline{\alpha}} -V(a, \beta_c(\alpha); \overline{\alpha}, \beta_*)\,\mathrm{d}a = \left[-\frac{1}{2}Bt\right]_{\alpha}^{\overline{\alpha}} + \int_{\alpha}^{\overline{\alpha}} t\left(\frac{\partial B}{\partial a} - \frac{3B}{2(a-b)}\right)\mathrm{d}a. \qquad (3.11)$$

In the integral of (3.11), t denotes $t(a, \beta_c)$ and $B \equiv B(a, \beta_c; \overline{\alpha}, \beta_*)$ and likewise for the derivative of B. The contributions from the segments CD and DA are, respectively, given by

$$\int_{\beta_c}^{\beta_*} U(\overline{\alpha}, b; \overline{\alpha}, \beta_*)\,\mathrm{d}b = \left[\frac{1}{2}Bt\right]_{\beta_c}^{\beta_*} \text{ and } \int_{\overline{\alpha}}^{\alpha_*} -V(a, \beta_*; \overline{\alpha}, \beta_*)\,\mathrm{d}a = \left[-\frac{1}{2}Bt\right]_{\overline{\alpha}}^{\alpha_*}. \qquad (3.12)$$

Finally, we evaluate the integral along the curve AB, which is parameterised as $\beta = \beta_c(\alpha)$ (and as $b = b_c(a)$). This yields

$$\int_{\alpha_*}^{\alpha}\left(-V + U\frac{\mathrm{d}b_c}{\mathrm{d}a}\right)\mathrm{d}a = \int_{\alpha_*}^{\alpha}\left[-\frac{3tB}{2(a-b_c)}(1+b_c') + t\frac{\partial B}{\partial a} + Bb_c'\frac{\partial t}{\partial b} - \frac{1}{2}\frac{\mathrm{d}}{\mathrm{d}a}(tB)\right]\mathrm{d}a. \qquad (3.13)$$

In this integral, the Riemann function $B \equiv B(a, b_c; \overline{\alpha}, \beta_*)$ and likewise for its derivatives, and the time field $t = (a + 3b_c)/4$. Then, after combining these contributions,

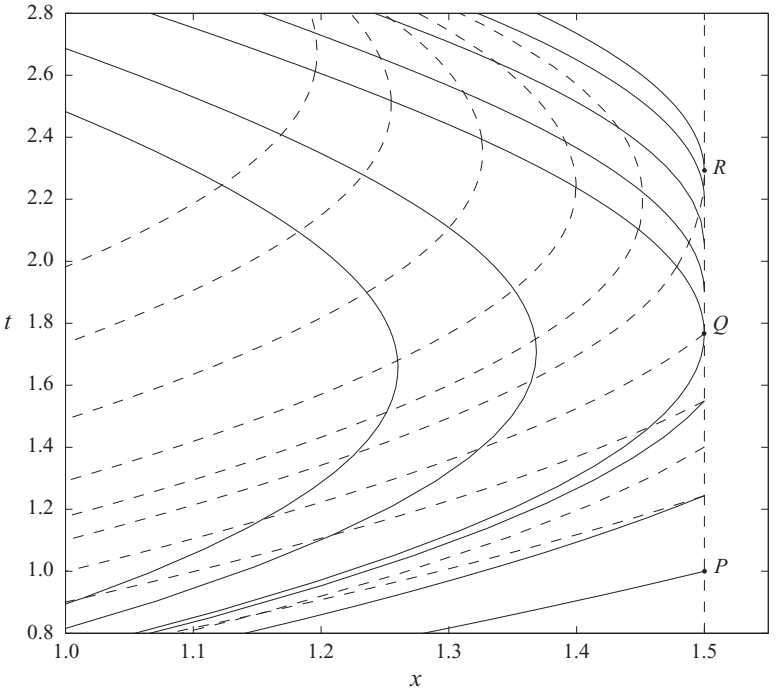

FIGURE 4. Characteristics in the (x, t) plane for $E = 1.5$, with α and β characteristics depicted by dashed and solid lines, respectively. The points $P = (E, t_s)$, $Q = (E, t_*)$ and $R = (E, t_f)$ represent the times at which there are different phases of the overtopping. At P, the lead characteristic first reaches $x = E$ and thereafter supercritical overtopping occurs, until the flow has sufficiently slowed and deepened. The Froude number at $x = E$ first drops to unity at point Q and thereafter the overtopping is controlled by a critical condition at $x = E$. At R, the shoreline begins to retreat and no further overtopping occurs.

using the boundary condition at $x = E$, we find that

$$0 = t(\overline{\alpha}, \beta_*) - \left(\frac{\overline{\alpha} - \beta_c}{\overline{\alpha} - \beta_*}\right)^{3/2} t(\overline{\alpha}, \beta_c) + \int_{\alpha}^{\overline{\alpha}} t\left(\frac{\partial B}{\partial a} - \frac{3B}{2(a - \beta_c)}\right) \mathrm{d}a + \int_{\alpha_*}^{\alpha} \left[-\frac{3tB}{2(a - b_c)}(1 + b_c') + t\frac{\partial B}{\partial a}\right] \mathrm{d}a. \quad (3.14)$$

Before we may evaluate this expression at points within the interior of the domain that are affected by the critical condition imposed at the end of the truncated beach, we must first determine the curve β_c. To this end, we let $\overline{\alpha} \to \alpha$ (i.e. the point C coincides with B) and on further substituting the condition of critical flow conditions, $t = (\alpha + 3\beta_c)/4$, we derive an integral equation for the curve representing $x = E$ in the hodograph plane, which is labelled AB in figure 3. This is given by

$$0 = t(\alpha, \beta_*) - \left(\frac{\alpha - \beta_c}{\alpha - \beta_*}\right)^{3/2} \left(\frac{\alpha + 3\beta_c}{4}\right) + \int_{\alpha_*}^{\alpha} \left(-\frac{3B}{2(a - b_c)}(1 + b_c') + \frac{\partial B}{\partial a}\right) \left(\frac{a + 3b_c}{4}\right) \mathrm{d}a. \quad (3.15)$$

This is an integral equation for $\beta_c(\alpha)$. It is most readily integrated numerically by differentiating with respect to α to give

$$3\beta_c' = 4\left(\frac{\alpha - b_*}{\alpha - \beta_c}\right)^{3/2}\frac{\partial t}{\partial \alpha} - \frac{9}{4}\frac{(\beta_c - \beta_*)(\alpha + 3\beta_c)}{(\alpha - \beta_*)(\alpha - \beta_c)} - 1 + \left(\frac{\alpha - \beta_*}{\alpha - \beta_c}\right)^{3/2}\int_{\alpha_*}^{\alpha}\left(-\frac{3}{2}\frac{(1 + b_c')}{(a - b_c)}\frac{\partial B}{\partial \alpha} + \frac{\partial^2 B}{\partial a \partial \alpha}\right)(a + 3b_c)\,\mathrm{d}a. \tag{3.16}$$

The equation is now in the form of a Volterra integral equation of the second kind, which may be solved numerically by iteration. Some numerical difficulties are experienced as the depth of fluid, measured by $\alpha - \beta$, becomes very small. To this end, it is simpler to perform the computations in a rotated coordinate system so that $\sigma = \alpha - \beta_c$ and $\lambda_c = \alpha + \beta_c$, and to determine the curve AB as a function of the parameter σ. This is possible provided that σ varies monotonically with α, a condition that has been confirmed numerically for $E > 1$. We denote the value of λ attained at $\sigma = 0$ by λ_f, noting that the time at the point, $t = t_f$, and the values of the characteristic variables, $\alpha = \alpha_f$ and $\beta = \beta_f$, are all equal to $\lambda_f/2$.

In the numerical computations, we calculate $\lambda_c(\sigma_i)$, where $\sigma_i = \sigma_*(1 - i/N)$ and find converged solutions to a relative accuracy of 10^{-6} with $N = 200$, typically after 10 iterations. As E is decreased towards unity, we need to use an increased resolution and more iterations to attain a converged solution.

We plot the solution for the curve in the hodograph plane in figure 3. For this calculation, we have assigned $E = 1.5$, but all values of $1 < E < 2$ have the same generic structure. It is straightforward to calculate the characteristic curves, given $t(\alpha, \beta)$ within the domain affected by the critical condition at the end of the beach. The position is given parametrically by integrating along β-characteristics that emanate from the curve $\beta = \beta_c$ at $x = E$. From (2.7), we find that

$$x(\overline{\alpha}) = E + \frac{3}{4}\beta_c\,[t(\overline{\alpha}) - t(\alpha)] + \frac{1}{4}\overline{\alpha}t(\overline{\alpha}) - \frac{1}{4}\alpha t(\alpha) - \frac{1}{2}[t(\overline{\alpha})^2 - t(\alpha)^2] - \int_{\alpha}^{\overline{\alpha}}\frac{1}{4}t\,\mathrm{d}a. \tag{3.17}$$

The characteristic curves are plotted in figure 4. The points P and Q in the physical plane correspond to points S and A, respectively, in the hodograph plane. The former represents the time at which the flow front first arrives at the end of the beach, whereas the latter represents the time at which the flow at the end of the beach first becomes critical. Profiles of the depth and velocity fields at various instances of time during the critical phase of overtopping are plotted in figure 5. We note that the condition of criticality at $x = E$ leads to a discontinuity in the gradients of the depth and velocity field that propagates from the end of the beach ($x = E$) back into the domain. The position of this discontinuity follows the $\beta = \beta_*$ characteristic. We also note that flow reversal occurs within the domain away from the end of the beach, while overtopping continues at $x = E$. Overtopping ceases when the depth of fluid and velocity first vanish.

3.3. *Overtopping fluxes*

To complete the calculation we calculate the volume of fluid per unit width that overtops the end of the truncated beach. This is given by

$$V = \int_{t_s}^{t_*} uh\,\mathrm{d}t + \int_{t_*}^{t_f} uh\,\mathrm{d}t. \tag{3.18}$$

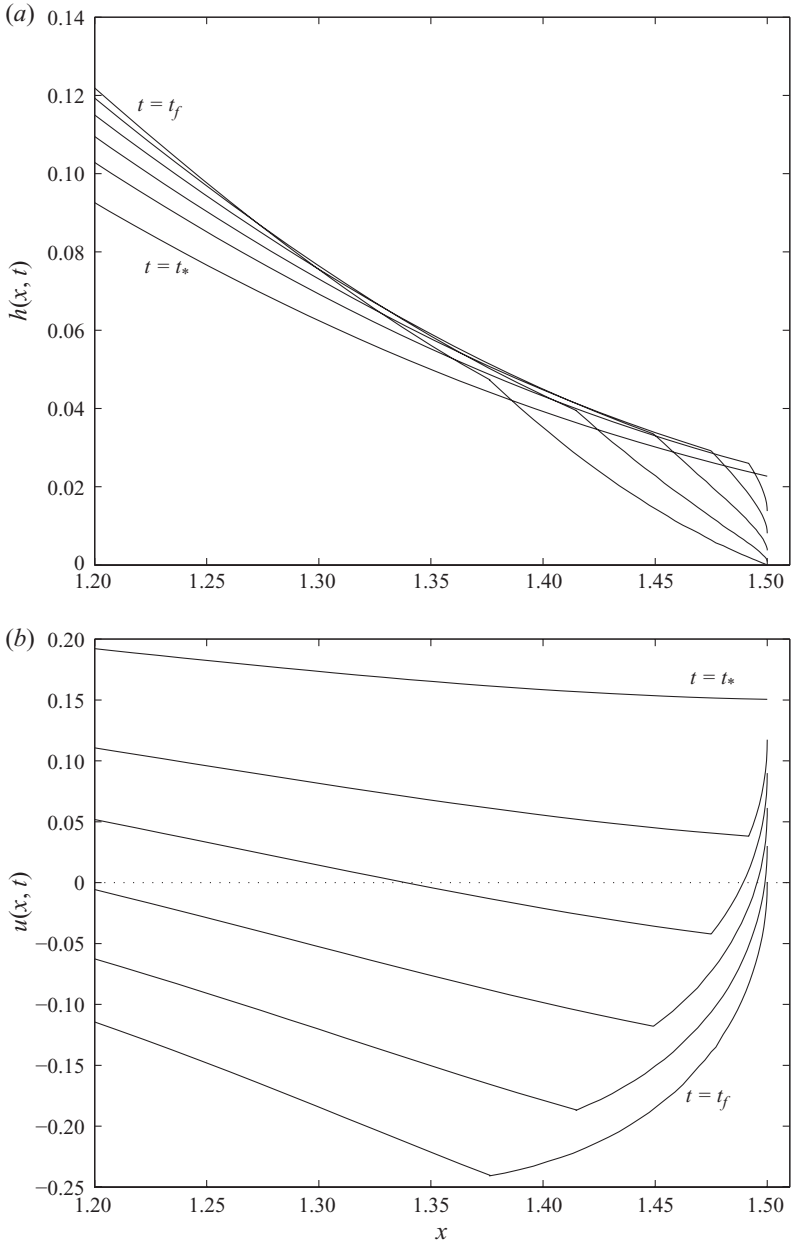

FIGURE 5. (*a*) The depth of fluid, $h(x, t)$, and (*b*) the velocity, $u(x, t)$, as functions of positions at $t = t_* = 1.767, 1.9, 2.0, 2.1, 2.2, t_f = 2.291$ during the critical phase of overtopping for $E = 1.5$. The first and last profiles are labelled; during this interval, the depth of fluid, $h(1.2, t)$, progressively increases and the velocity, $u(1.2, t)$, progressively decreases.

The first of these integrals, henceforth denoted by V_1, represents the volume flux during the supercritical phase of the overtopping motion. The second, henceforth denoted by V_2, represents the volume flux when the motion is critical at the end of

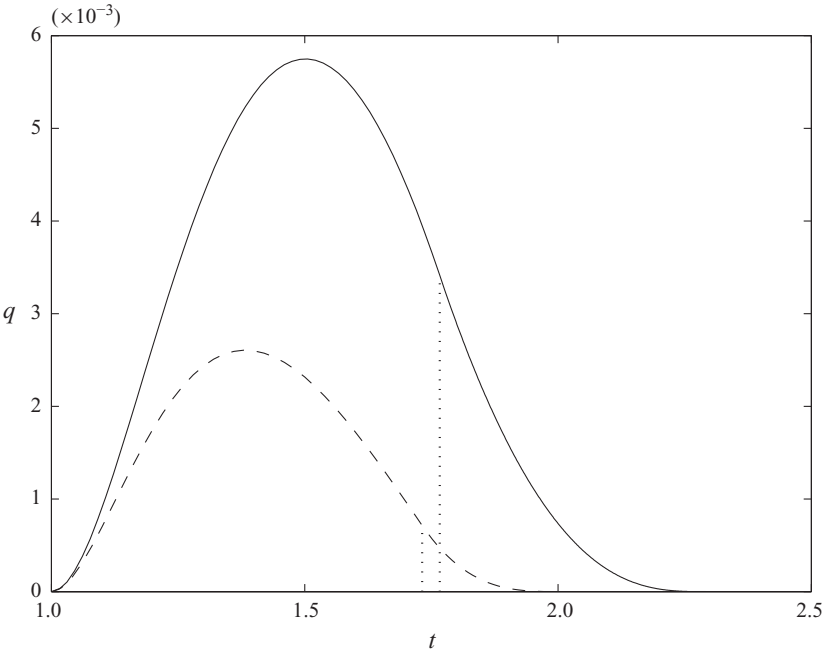

FIGURE 6. The volume flux per unit width at the end of the truncated beach, $q = u(E,t)h(E,t)$, as a function of time for the flow model employed in this study (solid line) and by Peregrine & Williams (2001) (dashed line), with $E = 1.5$ in each case. Also plotted are the times t_* at which the overtopping flow first becomes critical (dotted line).

the beach. Using the condition $u = \sqrt{h}$, it is given by

$$V_2 = \int_{t_*}^{t_f} \left(\frac{\alpha - \beta_c}{4}\right)^3 \mathrm{d}t \tag{3.19}$$

$$= \frac{\sigma_*^4}{1024} - \frac{\sigma_*^3 \lambda_*}{128} + \frac{3}{128}\int_0^{\sigma_*} \sigma^2 \lambda_c \,\mathrm{d}\sigma, \tag{3.20}$$

where $\sigma_* = \alpha_* - \beta_*$ and $\lambda_* = \alpha_* + \beta_*$.

In figure 6, we plot the temporal variation of the volume flux per unit width, $q = u(E,t)h(E,t)$ for $t_s < t < t_f$ for $E = 1.5$, showing the result from the calculation in this paper and from Peregrine & Williams (2001). We note that although the fluxes from both flows develop at the same time ($t_s = 1$) because the trajectories of the fronts are identical, the flux overtopping is greater for the fluid motion modelled in this paper and the flow recedes at a later time. This figure also illustrates some of the influence of the critical condition at the end of the beach: overtopping is finished at time t_f, which is before the retreat of the shoreline if the flow had been along an untruncated beach ($t = 2 + (4 - 2E)^{1/2}$). We also note that the flow develops a bore during the backwash on a beach without overtopping (Antuono & Hogg 2009), but that such a feature is not found during the overtopping of a truncated beach. In figure 7, we consider the variation of the total volume of fluid that overtops the beach with the dimensionless length of the beach. We note that the current model exceeds the predictions of Peregrine & Williams (2001) by an order of magnitude for relatively short beaches, but that the predictions converge as the dimensionless length of the beach approaches the maximum run-up distance of the incoming fluid

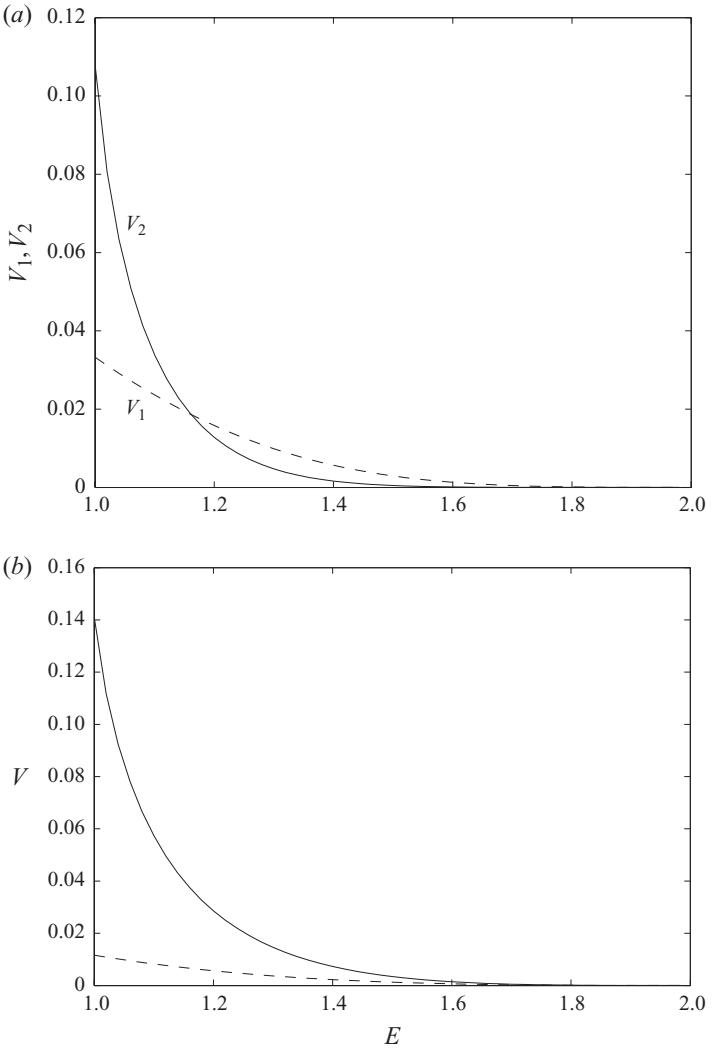

FIGURE 7. The volume of fluid per unit width overtopping the truncated beach. In (*a*) the overtopping volumes during the supercritical and critical phases are plotted (V_1 and V_2, respectively). In (*b*), the total overtopping volume is plotted (solid line), along with that calculated by Peregrine & Williams (2001) (dashed line).

($E \to 2$) and the overtopping volume vanishes. Indeed from the PW01 model, it may be shown that

$$V = \tfrac{1}{108}(2-E)^3 + \cdots \qquad \text{when} \quad 2-E \ll 1. \tag{3.21}$$

3.4. *Overtopping from dam-break flows with finite reservoirs*

Our calculations of overtopping volumes have thus far been for flows from reservoirs that are sufficiently long that the fluid has retreated from the end of the truncated

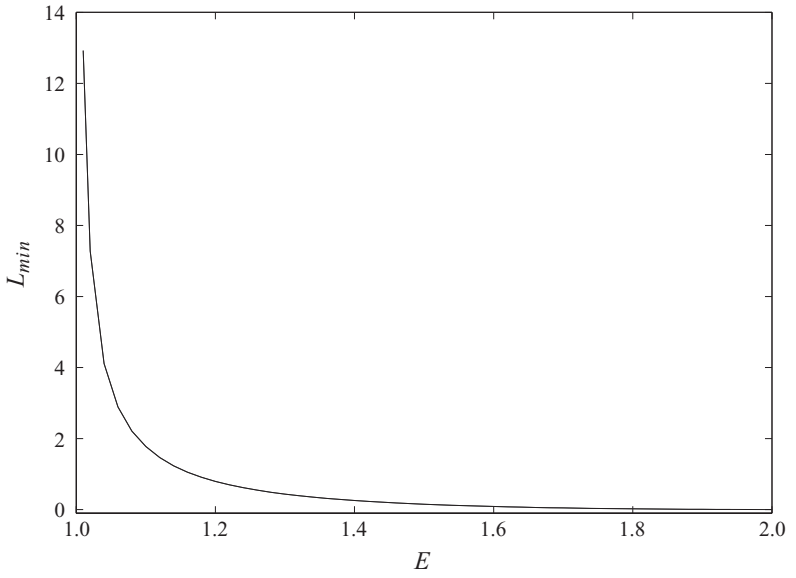

FIGURE 8. The minimum length of reservoir, L_{min}, such that overtopping the truncated beach is not affected by the impermeable back wall, plotted as a function of the length of the beach, E.

beach and the overtopping has finished before any influence of the finite size of the reservoir is felt. In terms of the characteristics underlying the governing equations, this requires that the flow recedes before the α-characteristic generated by the reflection at the back wall of the rearmost β-characteristic, which arises from the initiation of the flow, has reached the end of the beach. In terms of the hodograph plane, this requires that $\alpha_f < \alpha_{ws} \equiv 4(1+L)^{1/2} - 2$ (see the Appendix). Thus, for each length of beach E, we may determine the minimum length of reservoir, L_{min}, so that its finite extent exerts no influence on the overtopping (see figure 8). We note that when converted to dimensional length scales, this constraint may correspond to flume lengths that are prohibitively large for laboratory investigations (see §4). Thus, in this section, we investigate the overtopping that occurs from finite-length dam-break releases.

The calculation is made possible by coupling the analysis of overtopping (see above) with the analysis for a finite-length reservoir (see the Appendix). It is most readily explained by reference to the hodograph plane (see figures 9 and 10).

First, employing the notation introduced in the Appendix that the curve in the hodograph plane corresponding to $u(0,t)=0$ is denoted by $\alpha=\alpha_w(\beta)$, we examine when the wall curve is such that $\alpha_w' > 0$ for all $\beta > -2$ (figure 9). The first stage of the calculation is to find the portion of the curve in the hodograph plane that corresponds to critical conditions before the back wall exerts any influence on the motion ($\beta=\beta_c(\alpha)$ for $\alpha_* < \alpha < \alpha_{ws}$). This computation is described above (§3.2) and thereafter we may evaluate $t(\alpha_{ws}, \beta)$ for $\beta_* < \beta < \beta_c(\alpha_{ws})$ using (3.14). Subsequent overtopping is affected by the back wall, and by using (A 7), we evaluate $t(\alpha, \beta_*)$ for $\alpha > \alpha_{ws}$. To extend the portion of the critical overtopping curve, $\beta_c(\alpha)$, into $\alpha > \alpha_{ws}$, we must first find $t(\alpha, \beta_c(\alpha_{ws}))$. This is straightforwardly done by applying the Riemann method to the straight line segments that make up the closed curve $PQRS$ (see

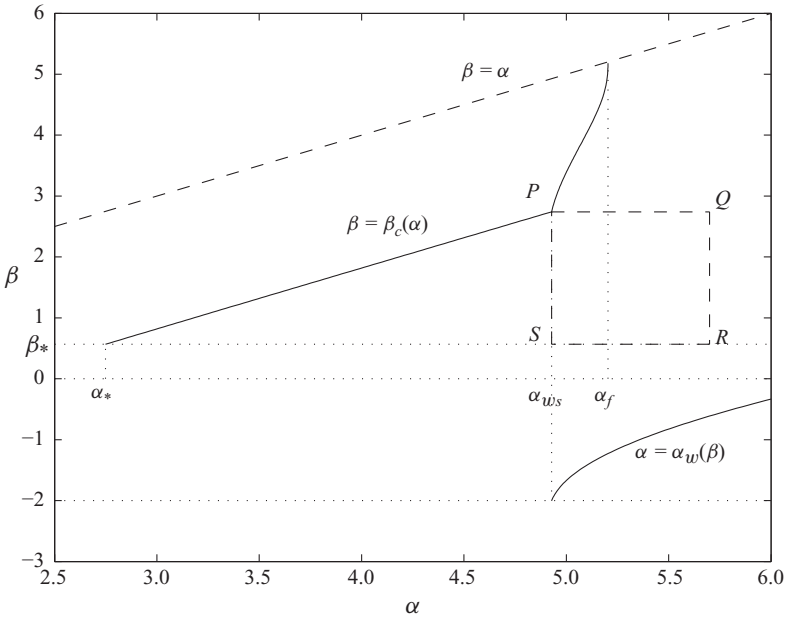

FIGURE 9. The hodograph plane for $L = 2$ and $E = 1$, showing the curve that represents the critical condition at the end of the truncated beach, $\beta = \beta_c(\alpha)$, and the curve that represents the no-flow condition at the back wall, $\alpha = \alpha_w(\beta)$. Critical conditions are first attained at the end of the beach when $\alpha = \alpha_*$ and the back wall begins to influence the flow when $\alpha = \alpha_{ws}$. For this length of reservoir ($L > L_c$), the hodograph plane does not develop a fold. Also shown is the integration contour $PQRS$, which is used to evaluate $t(\alpha, \beta_c(\alpha_{ws}))$.

figure 9), to yield

$$t(\alpha, \beta_c(\alpha_{ws})) = \left(\frac{\alpha_{ws} - \beta_c(\alpha_{ws})}{\alpha - \beta_c(\alpha_{ws})}\right)^{3/2} t(\alpha_{ws}, \beta_c(\alpha_{ws})) + \left(\frac{\alpha - \beta_*}{\alpha - \beta_c(\alpha_{ws})}\right)^{3/2} t(\alpha, \beta_*)$$
$$- B(\alpha_{ws}, \beta_*; \alpha, \beta_c(\alpha_{ws}))t(\alpha_{ws}, \beta_*) + \int_{\alpha}^{\alpha_{ws}} \left(\frac{\partial B}{\partial a} - \frac{3B}{2(a - \beta_*)}\right) t(a, \beta_*)\,\mathrm{d}a$$
$$+ \int_{\beta_*}^{\beta_c(\alpha_{ws})} \left(-\frac{\partial B}{\partial b} - \frac{3B}{2(\alpha_{ws} - b)}\right) t(\alpha_{ws}, b)\,\mathrm{d}b. \tag{3.22}$$

In the first of these integrals, $B \equiv B(a, \beta_*; \alpha, \beta_c(\alpha_{ws}))$ and likewise for its derivatives, while in the second, $B \equiv B(\alpha_{ws}, b; \alpha, \beta_c(\alpha_{ws}))$ and likewise for its derivatives. Armed with this evaluation of time along the β-characteristic $\beta = \beta_c(\alpha_{ws})$, it is then possible to extend the curve for critical overtopping using the methods described above (§§ 3.2 and 3.3). An illustrative plot is shown in figure 9. We note that the gradient of β_c is discontinuous at $\alpha = \alpha_{ws}$, reflecting the discontinuities in the gradients of the height and velocity fields across this characteristic.

The calculation is more complicated if $L < L_c$, thus implying that $\alpha_w'(-2) < 0$ and thus the hodograph plane develops folds (see figure 10). To proceed with the solution, we still need to evaluate $t(\alpha, \beta_c(\alpha_{ws}))$, which may be done using the methods presented earlier in this subsection, although, in this case, $\alpha_b < \alpha < \alpha_{ws}$, where α_b is the minimum value of $\alpha_w(\beta)$ (see the Appendix). Using this calculation, it is then possible to compute the extension of the critical curve in the hodograph plane. It is now possible that overtopping finishes ($\beta_c(\alpha) = \alpha$) for some value of α in

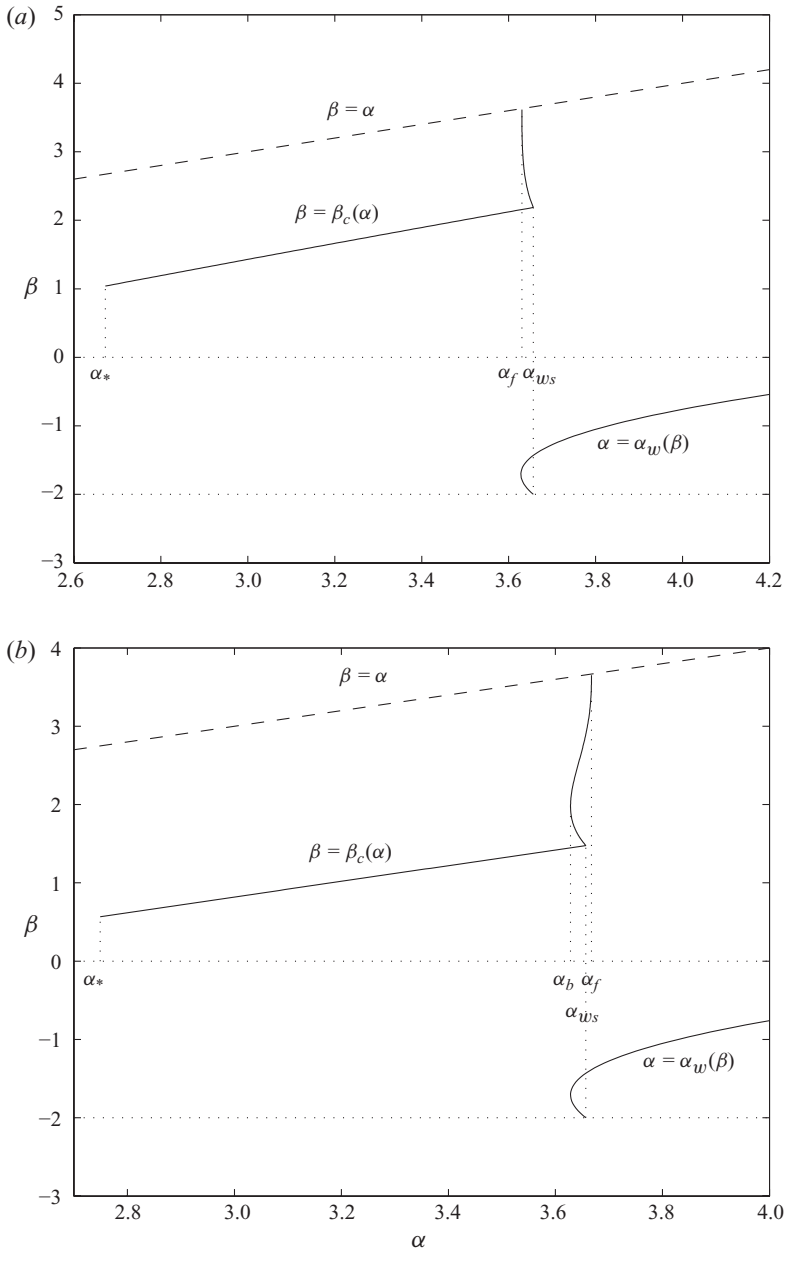

FIGURE 10. The hodograph plane for (*a*) $L=1$ and $E=0.9$, and (*b*) $L=1$ and $E=0.5$, showing the curve that represents the critical condition at the end of the truncated beach, $\beta=\beta_c(\alpha)$ and the curve that represents the no-flow condition at the back wall, $\alpha=\alpha_w(\beta)$. Critical conditions are first attained at the end of the beach when $\alpha=\alpha_*$ and the back wall of the reservoir begins to influence the flow when $\alpha=\alpha_{ws}$. For both these sets of parameter values, the hodograph plane develops a fold at $\alpha=\alpha_{ws}$ and α-characteristics carry diminishing values of α for some period. In (*a*) overtopping finishes before the values of α begin to increase again, whereas in (*b*) overtopping finishes after this point.

this range, in which case the calculation is complete. Alternatively it is possible that the curve reaches the values $\alpha = \alpha_b$ and is thereafter defined for increasing α. Negotiating this fold in the hodograph plane does not cause any difficulties in principle: the time $t(\alpha, \beta_c(\alpha_b))$ must be evaluated along the β-characteristic emanating from the turning point of the critical curve and then the same methods for finding the overtopping curve can be followed until the flow has receded from the end of the truncated beach. In figure 10, we plot the critical overtopping curve for both of these scenarios.

4. Experiments

Experiments to measure overtopping volumes from dam-break initial conditions were conducted in a tilting flume in the School of Civil Engineering, University of Queensland. A schematic of the experimental facility is shown in figure 1. The tilting flume is 3 m long, 0.4 m wide and 0.4 m high. The flume has an impermeable PVC bed (roughness height, $k_s \approx 0.01$ mm) and clear glass walls. One end of the flume ($x = -L$) is closed permanently. The other end is open to allow overtopping. A dam gate can be located at any position along the flume length to hold a reservoir of desired volume. The dam gate is PVC, 12 mm thick, with a silicon seal at the sides and a flexible foam seal at the base. The seals together with a small amount of silicon grease along the sidewall on the reservoir side eliminate sufficient leakage from the reservoir so that the bed downstream of the gate can be maintained as dry prior to the gate release. A small drain hole immediately downstream of the gate facilitates draining small leaks while filling the reservoir and setting instrumentation. The gate is raised by a pivoting lever arm and this was performed manually. Video analysis of the gate indicated that it opened to a height in excess of 0.2 m in approximately 0.12 s and thus following Lauber & Hager (1998), we anticipate that the speed of gate opening is sufficiently rapid for it to have little effect on the flow that ensures. Figure 11(a) shows the dry bed ahead of the fluid and a wall of water that is approximately perpendicular to the base of the flume at the instant the gate is clear of the water surface. Figure 11(b) illustrates the run-up flow tip during propagation up the slope towards the edge, showing that the fluid attains a smooth profile.

Overtopping experiments were performed for three different flume gradients, 1/10, 1/20 and 1/30. The reservoir length, L^*, was varied between 1 and 2 m, with initial water depths, h_0^*, behind the dam ranging from 0.055 to 0.28 m. Flow depths were measured approximately 6 cm back from the edge and at the mid-point of the channel using non-intrusive Mic+25 Microsonic acoustic displacement sensors. A further sensor was attached to the gate to provide a timing trigger. Overtopping flow was collected in overtopping tanks of different sizes, from which the overtopping volumes were obtained. Secondary and reflected waves from the back wall result in a sequence of overtopping events in general. To ensure that only the initial overtopping event was measured, a flap hinged to the upper part of the flume at the open edge was closed manually the instant the initial overtopping ceased, excluding secondary waves from the measured volumes.

Previous experimental studies of the run-up of fluid from dam-break initial conditions in this experimental configuration (Baldock *et al.* 2007) revealed that the maximum run-up was significantly less than the theoretical dimensional maximum of $2h_0^*/\tan\theta$. This difference is presumably due to the action of drag on the thin layer of fluid at the front of the flow. Therefore, we were unable to study truncated beaches of dimensionless lengths, $E > 1.2$, because the fluid does not run up beyond that point. However, it also emerged that all bar one of the experimental

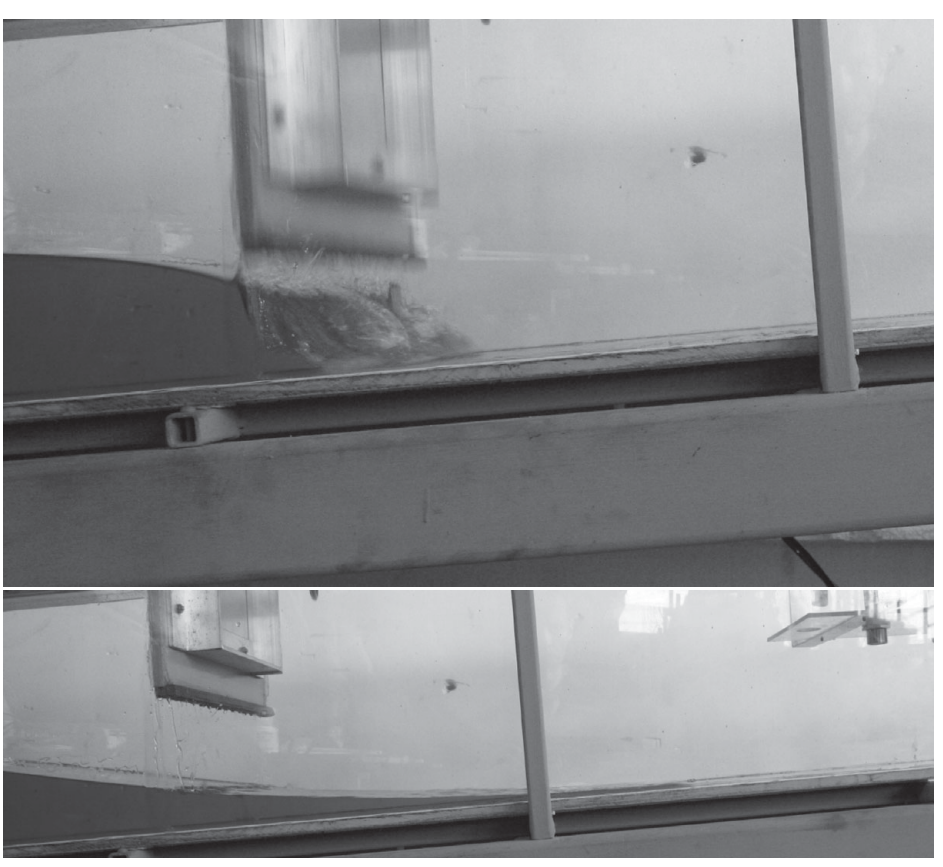

FIGURE 11. Photographs of dam-break flows in the laboratory flume for conditions $h_0 = 0.1$ m, $L^* = 1.6$ m and $\tan\theta = 0.1$. The photographs show the fluid (*a*) just after the gate has cleared the reservoir of fluid and (*b*) when the wavefront is approximately halfway through its run-up.

conditions were affected by the presence of the back wall, measured in dimensionless terms by $L < L_{min}$ (see figure 8). This is an important conclusion about this set of experiments, illustrating the need for the calculations in the Appendix; many of the experimental conditions were for relatively short truncated beaches ($E < 1$) for which the overtopping volume from an unbounded reservoir would be infinite. The dimensionless length of the beach, E, ranged between 0.17 and 1.22, while the dimensionless length of the reservoir, L, ranged between 0.33 and 2.38. We report the experimental conditions and the theoretical predictions in table 1.

For each set of values for the dimensionless lengths of the beach and the reservoir, we compute the theoretical predictions for the dimensionless overtopping volume per unit width and we plot the theoretically calculated and experimentally measured results in figure 12 and give the numerical values in table 1. We note that there is generally good quantitative agreement between the theory and the experiments. There are some outliers for which the theory overpredicts the experimentally measured values. These are associated with relatively long beaches (often with $E \gtrsim 1.0$) and long reservoirs, for which drag curtails the overtopping earlier than predicted by the inviscid model. The remaining outlier, which is an underprediction by the model, corresponds to the experimental conditions with the greatest reservoir depth (and maximum

$\tan\theta$	L^* (m)	E^* (m)	h_0^* (m)	Volume (m^3)	L	E	V_{exp}	V	$\hat{V}$
0.100	1.0	2.0	0.248	0.0173	0.403	0.810	0.070	0.080	0
0.100	1.0	2.0	0.220	0.0109	0.455	0.914	0.056	0.069	0
0.100	1.0	2.0	0.200	0.0065	0.500	1.005	0.040	0.057	0
0.100	1.0	2.0	0.190	0.0050	0.526	1.058	0.035	0.050	0
0.100	1.0	2.0	0.165	0.0004	0.606	1.218	0.004	0.025	0
0.100	2.0	1.0	0.187	0.0436	1.070	0.537	0.312	0.304	0.350
0.100	2.0	1.0	0.152	0.0232	1.316	0.661	0.251	0.275	0.227
0.100	2.0	1.0	0.103	0.0028	1.942	0.976	0.067	0.125	0
0.100	2.0	1.0	0.084	5.7×10^{-6}	2.381	1.196	2.0×10^{-4}	0.029	0
0.050	2.0	1.0	0.275	0.1659	0.364	0.182	0.274	0.217	0.281
0.050	2.0	1.0	0.200	0.0872	0.500	0.250	0.272	0.260	0.344
0.050	2.0	1.0	0.158	0.0594	0.633	0.317	0.298	0.287	0.382
0.050	2.0	1.0	0.100	0.0238	1.000	0.501	0.297	0.309	0.374
0.050	2.0	1.0	0.055	0.0011	1.818	0.910	0.047	0.162	0
0.050	1.0	2.0	0.148	0.0142	0.338	0.677	0.081	0.090	0
0.050	1.0	2.0	0.100	0.0006	0.500	1.001	0.007	0.057	0
0.033	2.0	1.0	0.072	0.0170	0.926	0.463	0.273	0.310	0.390
0.033	2.0	1.0	0.050	0.0068	1.333	0.667	0.226	0.274	0.221
0.033	2.0	1.0	0.102	0.0345	0.654	0.327	0.277	0.291	0.386
0.033	2.0	1.0	0.150	0.0685	0.444	0.222	0.254	0.245	0.321
0.033	2.0	1.0	0.200	0.0843	0.333	0.167	0.176	0.207	0.264

TABLE 1. The experimental measurements of the overtopping volumes resulting from dam-break initial conditions, along with the dimensionless length of reservoir, L, distance to the end of the beach, E, and experimentally determined dimensionless overtopping volume, V_{exp}. Also listed are the theoretical predictions of the dimensionless volume per unit width, V, and the simple estimate, $\hat{V} = \max(0, (1/2)(2+L)L - (1/2)(L+E)^2)$.

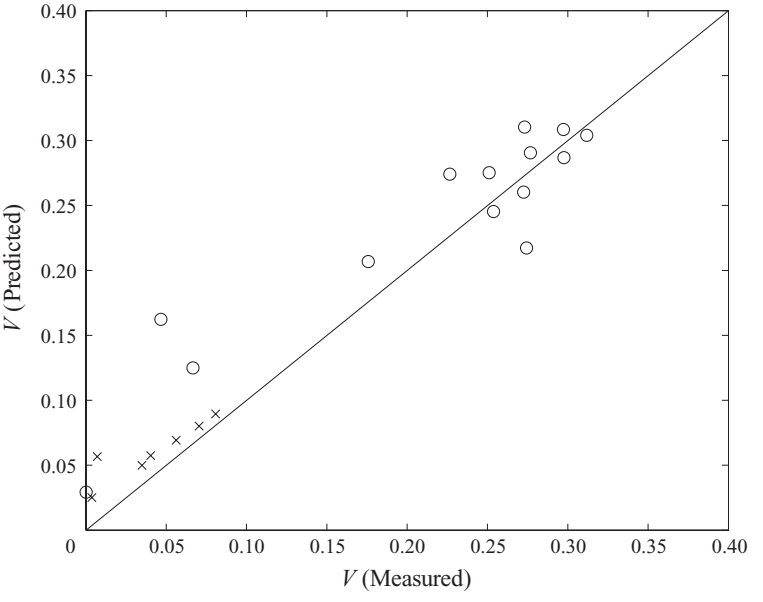

FIGURE 12. The theoretical predictions of the dimensionless overtopping volume per unit width plotted against the experimentally measured values. Data were collected at various inclinations of the flume, depths of fluid behind the dam and lengths of reservoir ($\times$ $L^* = 1$ m; $\circ$ $L^* = 2$ m). The solid line represents perfect agreement.

dimensional overtopping). It is possible that the finite gate opening time is a reason for this mismatch between theory and experimental measurements, because it changes the nature of the initial wave that propagates towards the back wall and its subsequent reflection. However, notwithstanding these discrepancies, the agreement between the predicted and observed volumes, with no empirically determined fitting parameters, is encouraging and is supportive of the framework for modelling overtopping developed in this study. In particular, the experimental results indicate that the shallow-water equations, coupled to the condition of hydraulic control, are able to predict accurately the overtopping volumes. Also given in table 1 is a calculation of overtopping volumes just based on conservation volumes: the overtopping volume is estimated as the difference between the initial fluid volume and the volume that could be contained within the flume when the fluid is quiescent with a horizontal surface, having spread along the entire length of the apparatus. This dimensionless overtopping volume per unit width is then calculated as $\hat{V} = \max(0, (2+L)L/2 - (L+E)^2/2)$. Although this simple prediction is in reasonable accord with the experiments when the distance to the end of the flume is very short ($E \ll 1$), it fails to account for the flow dynamics that lead to run-up and overtopping for longer beaches ($E = O(1)$).

5. Overtopping from Guard–Baldock waveforms

In this section, we calculate the overtopping under the model of wave run-up on a linear beach introduced by Guard & Baldock (2007) and subsequently written in analytical form by Pritchard *et al.* (2008).

The solution developed by Guard & Baldock (2007) is constructed as a generalisation of the 'dam-break' solution of Shen & Meyer (1963), with a single additional adjustable parameter. As in a dam-break flow, the initial condition involves the collapse of a vertical front at $(x, t) = (0, 0)$, creating a 'fan' of β-characteristics. A seaward boundary condition is subsequently imposed in which the incoming characteristic information α increases with time, rather than remaining constant, $\alpha = 2$, as in the Shen & Meyer solution. This represents a more sustained incoming flux of fluid, typical of a developed bore in which the incoming water has some onshore momentum at time $t = 0$; the result is that the swash lens becomes deeper and the on- and offshore velocities more symmetrically distributed either side of flow reversal than in the Shen & Meyer solution.

Specifically, for convenience, the solution of Guard & Baldock (2007) employs the boundary condition $\alpha = 2 + kt$ on the retreating characteristic $\beta = -2/3$ (which corresponds to the back of the characteristic fan). The limit $k = 0$ corresponds to the Shen & Meyer solution; as k is increased, the bore is sustained more strongly, and Guard & Baldock (2007) demonstrated that $k = 1$ gave reasonably good agreement with experimental measurements of the depth within the swash zone.

In terms of the hodograph variables, Pritchard *et al.* (2008) showed that

$$t = \frac{1}{k}\int_2^{\alpha} \frac{5a - \dfrac{14}{3}}{2\left(a + \dfrac{2}{3}\right)} B\left(a, -\frac{2}{3}; \alpha, \beta\right) \mathrm{d}a, \tag{5.1}$$

and $x(\alpha, \beta)$ is given by (3.2). This solution develops the same motion at its front as that formed by the flow with dam-break initial conditions, namely $x_f = 2t - (1/2)t^2$ (which corresponds to the characteristic variables $\alpha = \beta = 2$).

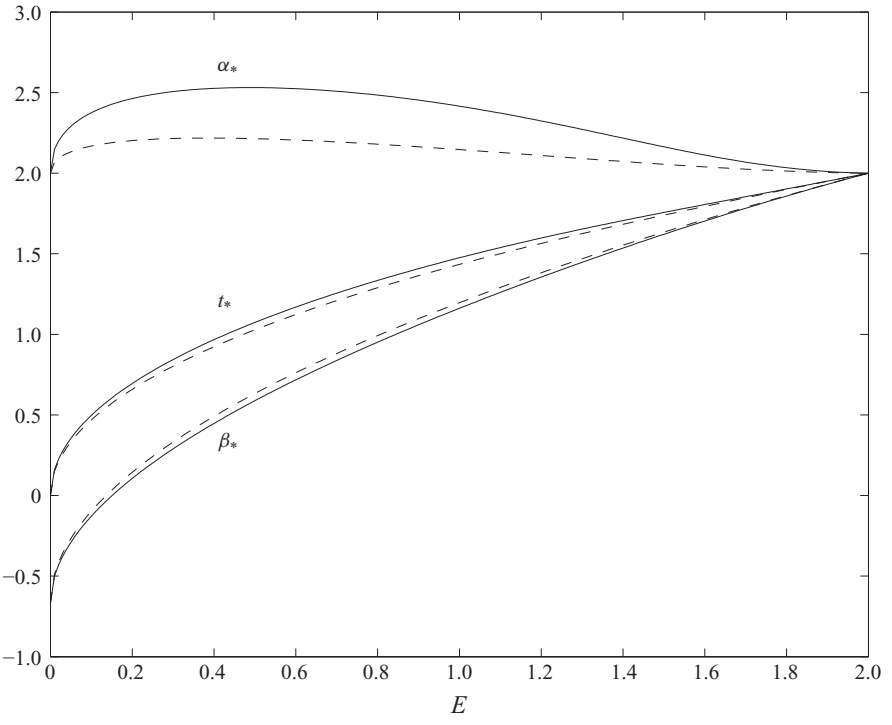

FIGURE 13. The values of the characteristic variables, α_* and β_*, and the time, t_*, at which critical conditions are first attained at the end of the truncated beach as functions of the length of the beach, E, for the model of wave run-up given by Pritchard *et al.* (2008) with $k = 0.5$ (dashed line) and 1 (solid line).

We may now use this model of wave run-up to determine the volume of fluid per unit width that overtops a truncated beach of length E. To this end, we find that the flow first reaches the end of the beach at $t = t_s \equiv 2 - \sqrt{4 - 2E}$ (see (3.4)). The flow remains supercritical until $u = \sqrt{h}$ at $x = E$ and this first occurs at $(t, \alpha, \beta) = (t_*, \alpha_*, \beta_*)$. We plot these quantities as functions of the length of the beach in figure 13. Thereafter, the overtopping flow remains critical until the flow recedes at $t = t_f$, a time that is determined as part of the solution.

During the phase of critical overtopping, we calculate the evolution using the analytical framework presented above (§ 3.2). In particular, we calculate the curve in the hodograph plane, $\beta_c(\alpha)$, along which $x = E$. This is equivalent to the curve AB in figure 3, but is now computed from the integral (3.15), using the flow field given by (5.1). Given this, we now compute the volume of fluid per unit width, V, that overtops the truncated beach for $k = 1$ and $k = 0.5$ (see figure 14). We note that we have calculated finite volumes for all values of $0 < E < 2$, in contrast to the overtopping generated by the dam-break initial conditions, because the fluid motion modelled by (5.1) eventually recedes fully from the beach.

As k increases and the bore is more strongly sustained, greater volumes of fluid overtop the beach. For moderate values of E, i.e. $2 - E = O(1)$, taking $k = 1$ (the best fit to experimental data for long solitary bores) rather than $k = 0$ (the Shen–Meyer solution) increases the predicted overtopping volume by a factor of roughly 3.

The effect of varying k is strongest for higher values of k, reflecting the nonlinear relationship between the value of k and the total amount of fluid which enters the

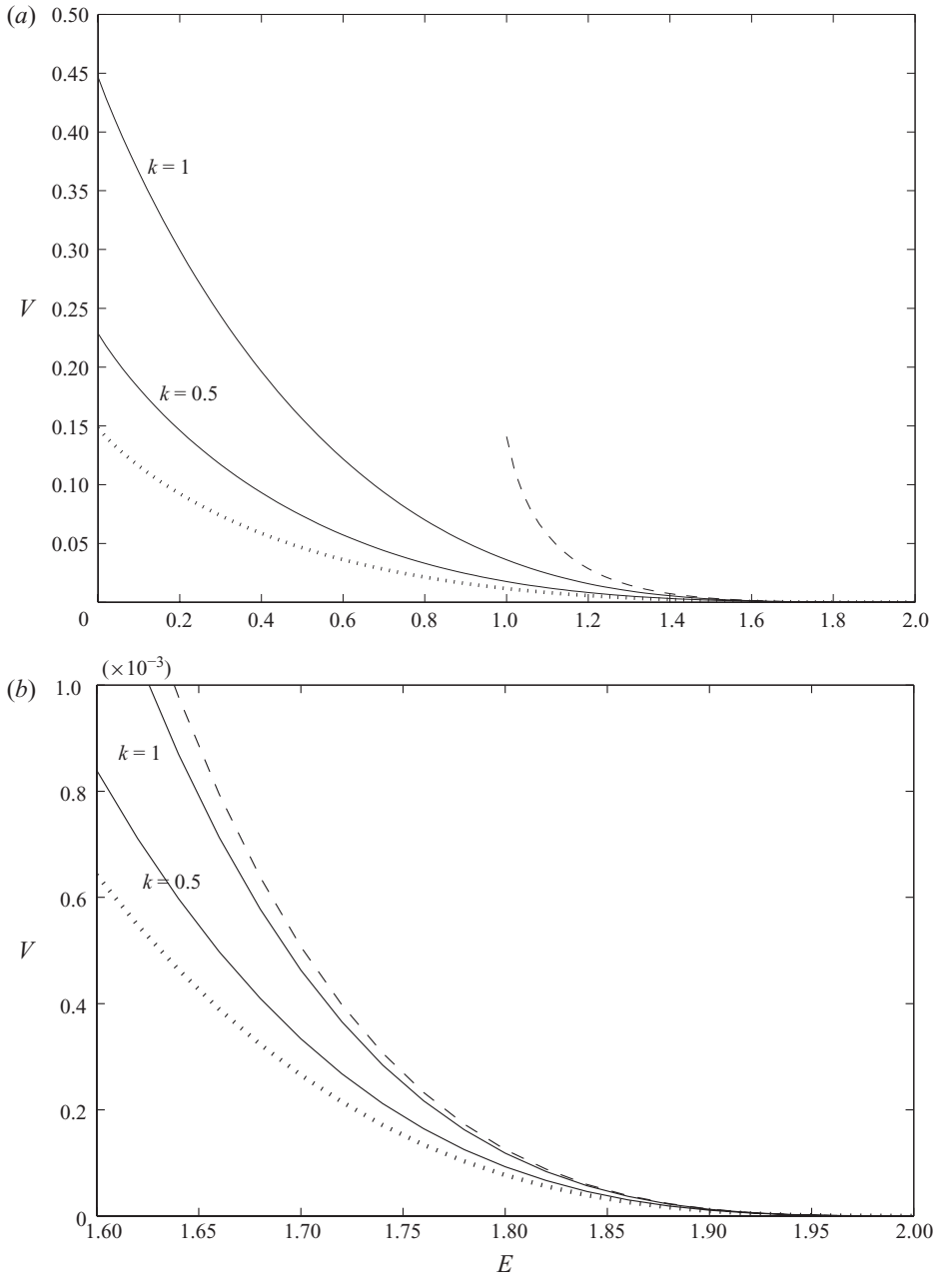

FIGURE 14. The volume of fluid per unit width that overtops the truncated beach as a function of the length of the beach, E, for the model of wave run-up given by Pritchard *et al.* (2008) with $k = 0.5$ and 1. Also plotted is the overtopping volume per unit width associated with dam-break flow (dashed line) and the overtopping calculated by Peregrine & Williams (2001) (dotted line). In (*b*) the results are viewed as plotted in the regime $2 - E \ll 1$.

swash zone (Pritchard *et al.* 2008). For values of E closer to $E = 2$, the value of k is less important, because solutions with any value of k are asymptotic to the Shen–Meyer solution with $k = 0$. However, it is important to note that in this regime, in practice drag is likely to become important.

Even the strongly sustained bore with $k = 1$ predicts significantly lower overtopping volumes for moderate values of E than does the dam-break solution presented in § 3. This reflects the fact that dam-break with an infinite reservoir can be regarded as, effectively, an indefinitely sustained offshore bore, which maintains the overtopping flow for longer (and indeed, for $E < 1$, maintains it indefinitely so V becomes undefined).

6. Summary and conclusions

In this contribution, we have applied the nonlinear shallow-water equations, coupled with the condition of hydraulic control at the end of the truncated beach to calculate the volumes of fluid per width that overtop for individual swash events. Specifically we have analysed the overtopping due to the flows generated from dam-break initial conditions and from the waveform recently identified by Guard & Baldock (2007) to provide a good model of bore-driven swash. We typically find that the overtopping volumes per unit width far exceed the calculations of Peregrine & Williams (2001), by factors in excess of 10 in some situations. This difference occurs because the earlier contribution was built upon the hydrodynamic model of swash motion proposed by Shen & Meyer (1963), a model that provides an asymptotic representation of the flow field close to the front of the swash flow but does not account for fluid motion behind it. Thus, when the length of the truncated beach is close to the maximum run-up of the swash event, the calculations of Peregrine & Williams (2001) provide an asymptotic representation of the overtopping volumes, but for shorter beaches, they significantly underestimate this volume.

Our calculations for the overtopping volumes resulting from flows generated by dam-break initial conditions, extended to account for a finite reservoir length, were compared quantitatively to results from new laboratory experiments in exactly the same configuration. We showed that the agreement between the theoretical prediction and the experimental measurement was generally good, supporting the modelling framework developed in this study, although the predictions and measurements begin to diverge when $E \gtrsim 1.0$. We reiterate that there are no empirical or 'fitting' parameters introduced for this comparison. The experiments did, however, reveal an important dynamical feature that is not currently included in the model, namely the role of hydrodynamic drag. This leads to a slight overprediction of overtopping volumes, but more significantly it reduces the maximum run-up that may be attained by a single event. At the laboratory scales that we investigated, the maximum run-up was reduced by approximately 40 % from its theoretical value. If hydraulic drag were modelled using a quadratic drag law with a Chezy drag coefficient, C_D, then in terms of the dimensionless variables used in this study, it would introduce an extra term to the right-hand side of (2.1), given by $\Lambda u^2/h$, with the parameter $\Lambda = C_D/\tan\theta$ ranging from 10^{-2} to 10^{-1} in these experiments and drag would be non-negligible close to the front of the motion. Dam-break flows over horizontal surfaces also exhibit a drag-affected region close the front, the magnitude of which depends on $C_D^{1/3}$ (Hogg & Pritchard 2004*a*). Thus, if the same asymptotic structure persists for flows up inclined planes, then we might expect corrections to the drag-free velocities of order $(C_D/\tan\theta)^{1/3}$, which would lead to the significant curtailing of run-up.

Finally, we remark that this study has demonstrated another application of the analytical techniques that are possible once hodograph variables have been adopted. The determination of the structure of the characteristic plane offers considerable insight to the dynamics, especially concerning the onset of critical conditions at the

end of the truncated beach and the subsequent impact that this point of hydraulic control has on the rest of the flow, and the effects of the back wall of the reservoir when the fluid is released from dam-break initial conditions. The method typically yields integral equations that are readily integrated numerically. These results could have been computed using other strategies, such as a direct numerical integration of the governing equations, but these approaches would not have drawn out the structure of the characteristic plane as clearly. Our results can therefore be used as a test case for future numerical strategies.

The authors thank R. Grayson and B. Torr for assistance with the experiments and P. Guard and M. Barnes for providing the photographic images in figure 11. T.B. gratefully acknowledges support from the Australian Research Council and the CSIRO Wealth from Oceans Program. The authors also acknowledge the contributions of three anonymous referees, whose suggestions have led to many improvements of this paper.

Appendix. The effects of a finite reservoir on a dam-break flow

In this appendix, we investigate the change to the dam-break solution developed by Antuono & Hogg (2009) and used in § 3.1, induced by the presence of an impermeable back wall at $x=-L$. The effects of this boundary first begin to play a role in the motion when the rearmost characteristic bounding the fan region, and initiated from the origin at $t=0$, reaches $x=-L$. This occurs at $t\equiv t_{ws}=2(1+L)^{1/2}-2$. Furthermore, because this rearmost characteristic corresponds to $\beta=-2$ and because $u=0$ at the wall, we deduce that $\alpha\equiv\alpha_{ws}=4(L+1)^{1/2}-2$. Thereafter the effects of having removed the dam and initiated the flow at $t=0$ are felt throughout the entire fluid domain and we must explicitly enforce the condition that $u=0$ at $x=-L$; at times before t_{ws}, this was not necessary because the fluid in a region adjacent to the wall was stationary and the rearmost characteristic from the origin had not yet reached the wall. In terms of the hodograph plane, this means that there is no longer the boundary $\beta=-2$ to the region of moving fluid; rather this boundary is now a curve in the hodograph plane that must be calculated as part of the solution (see figure 15).

Our method follows Kerswell (2005), although the details are rather different because the initial condition for this flow is different. It is convenient to parameterise the curve in the hodograph plane as $\alpha=\alpha_w(\beta)$ and thus the conditions at the wall are

$$t=\tfrac{1}{2}(\alpha_w+\beta)\quad\text{and}\quad x=-L. \tag{A 1}$$

Differentiating these conditions with respect to β and for the second of them simplifying using the characteristic equations (2.6) and (2.7) and $u=0$, we find that

$$\frac{\mathrm{d}t}{\mathrm{d}\beta}=\frac{\partial t}{\partial\alpha}\alpha_w'+\frac{\partial t}{\partial\beta}=\frac{1}{2}(\alpha_w'+1)\quad\text{and}\quad\frac{\mathrm{d}x}{\mathrm{d}\beta}=0=-\frac{\partial t}{\partial\alpha}\alpha_w'+\frac{\partial t}{\partial\beta}, \tag{A 2}$$

where $\alpha_w'\equiv\mathrm{d}\alpha_w/\mathrm{d}\beta$. Thus, we find that along the curve that represents the boundary at the rear wall

$$\alpha_w'\frac{\partial t}{\partial\alpha}=\frac{\partial t}{\partial\beta}=\frac{1}{4}(\alpha_w'+1). \tag{A 3}$$

The first forward-propagating α-characteristic that is affected by the condition of no flow at $x=-L$ carries the value $\alpha\equiv\alpha_w(-2)=\alpha_{ws}$. It separates the fan region, within

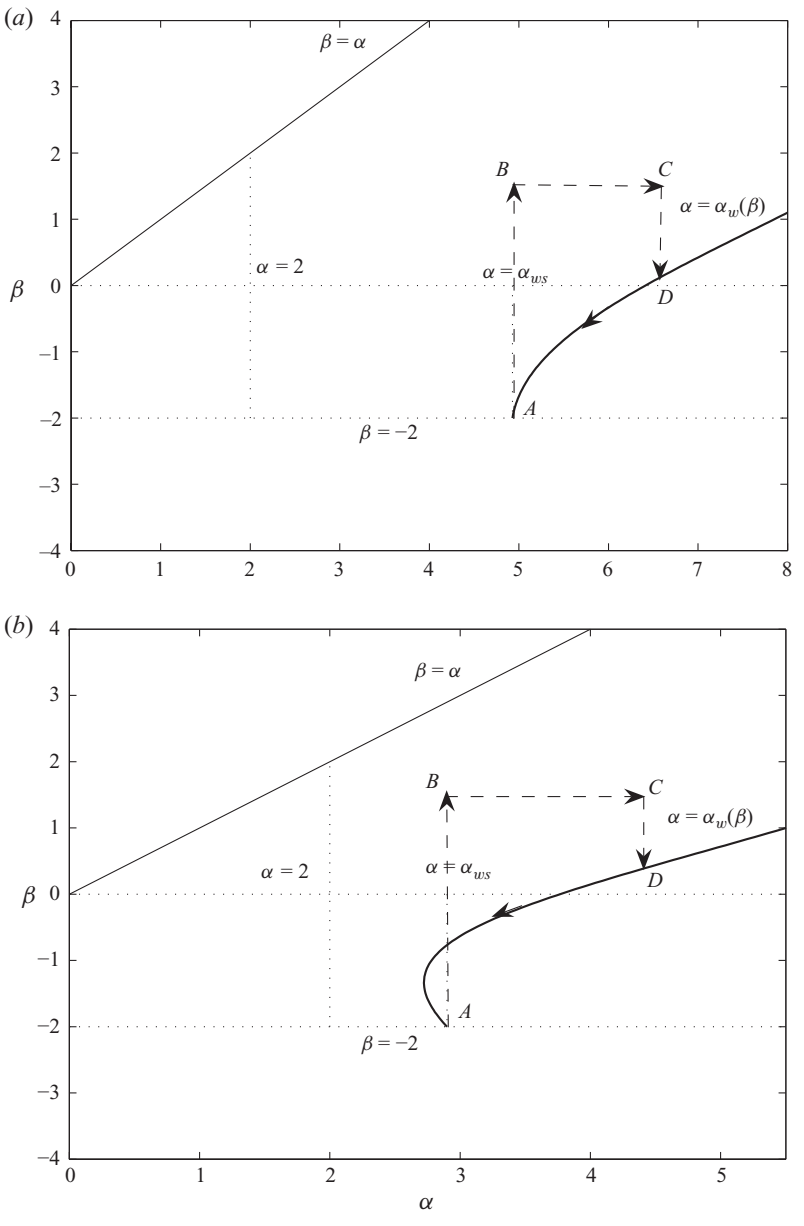

FIGURE 15. The hodograph plane for finite dam-break flows: (*a*) $L=2$; (*b*) $L=0.5$. The flow is given by the fan solution of (3.1) and (3.2), which is valid for $-2 \leqslant \beta \leqslant \alpha$ upto $\alpha = \alpha_{ws}$. at which point the rearmost β-characteristic reaches the back wall. Thereafter the position of the back wall corresponds to $\alpha = \alpha_w(\beta)$. Note that for (*b*), $L < L_c$ and $\alpha_w'(-2) < 0$, and this implies that the hodograph plane develops a fold. In both figures, $ABCD$ represents the integration contour employed to construct the solution.

which the solution is affected only by the removal of the dam at $x=0$ and is given by (3.1), from the region that is influenced by the impermeable back wall and which is analysed in this appendix. Time is continuous across this α-characteristic, as is the derivative along it ($\partial t/\partial\beta$). The normal derivative ($\partial t/\partial\alpha$) is, however, discontinuous across it.

From (3.1), we find that

$$\left.\frac{\partial t}{\partial \beta}\right|_{\beta=-2} = \frac{1}{2} - \frac{4}{(\alpha+2)^{3/2}} = \frac{1}{2}\left(1 - \frac{1}{(1+L)^{3/4}}\right), \tag{A 4}$$

on substituting $\alpha = \alpha_{ws}$. Further, using (A 3), we find that

$$\alpha_w'(-2) = \frac{(1+L)^{3/4}-2}{(1+L)^{3/4}} \quad \text{and} \quad \left.\frac{\partial t}{\partial \alpha}\right|_{\beta=-2} = \frac{(1+L)^{3/4}-1}{2((1+L)^{3/4}-2)}, \tag{A 5}$$

the latter showing that the value of $\partial t/\partial\alpha(\beta=-2)$ varies discontinuously across this α-characteristic from the value of $1/2$ within the fan. Thus, we deduce that if $L < L_c \equiv 2^{4/3} - 1$, then $\alpha_w'(-2) < 0$ and so the hodograph plane develops a fold. This means that there are forward-propagating α-characteristics that are associated with $\alpha < \alpha_{ws}$. This also shows why it is convenient to parameterise this boundary curve as a function of β, because for $L < L_c$, there is a point along the curve at which $\alpha_w' = 0$, and this would have introduced a singularity in the calculations had we parameterised the curve as a function of α.

To calculate the curve and the solution affected by the back wall, we employ Riemann's method and integrate around a closed curve in the hodograph plane using the identity given by (2.14). Our closed curve connects the points A, B, C and D, given by

$$A = (\alpha_{ws}, -2), \qquad B = (\alpha_{ws}, \hat{\beta}), \qquad C = (\alpha_w(\beta), \hat{\beta}) \quad \text{and} \quad D = (\alpha_w(\beta), \beta), \tag{A 6}$$

and depicted in figure 15. The segments AB, BC and CD are straight lines, while DA is along the curve $\alpha = \alpha_w(\beta)$. This closed contour may be used straightaway when $L > L_c$. However, when $L < L_c$, there exists a point at which $\alpha_w' = 0$ and thus the hodograph plane develops folds that require more careful negotiation, as described below. Using the closed curve $ABCD$, we find that

$$0 = t(\alpha_{ws}, \hat{\beta}) - \left(\frac{\alpha_w - \hat{\beta}}{\alpha_{ws} - \hat{\beta}}\right)^{3/2} t(\alpha_w, \hat{\beta}) + \int_{\hat{\beta}}^{\beta} \left[\frac{-3B}{2(\alpha_w - b)} - \frac{\partial B}{\partial b}\right] t(\alpha_w, b)\,\mathrm{d}b + \int_{-2}^{\beta} \left[\frac{3tB}{2(a_w - b)}(a_w' + 1) + t\frac{\partial B}{\partial b} + \frac{B}{4}(a_w' + 1)\right] \mathrm{d}b. \tag{A 7}$$

In the first integral of this expression, $B \equiv B(\alpha_w, b; \alpha_{ws}, \hat{\beta})$ and likewise for its derivatives; in the second integral, $B \equiv B(a_w(b), b; \alpha_{ws}, \hat{\beta}))$ and likewise for its derivatives, where $a_w(b)$ corresponds to $\alpha_w(b)$ and $t \equiv t(a_w, b)$. We now set $\hat{\beta} = \beta$ and identify $t(\alpha_w, \beta) = (\alpha_w + \beta)/2$, the latter representing the dependence of time along the curve in the hodograph plane representing $x = -L$ (see (A 1)). Thus, we find that

$$0 = t(\alpha_{ws}, \beta) - \left(\frac{\alpha_w - \beta}{\alpha_{ws} - \beta}\right)^{3/2} \frac{\alpha_w + \beta}{2} + \int_{-2}^{\beta} B\frac{(a_w' + 1)}{4}\left(\frac{3(a_w + b)}{a_w - b} + 1\right) + \frac{(a_w + b)}{2}\frac{\partial B}{\partial b}\,\mathrm{d}b. \tag{A 8}$$

This is an integral equation for the curve $\alpha_w(\beta)$. Below it is shown that this equation is readily integrated numerically by differentiating to form a Volterra equation and then treated using successive iterations. However, before tackling this, we return to the case $L < L_c$ for which $\alpha_w'(-2) < 0$. This means that the hodograph plane first develops

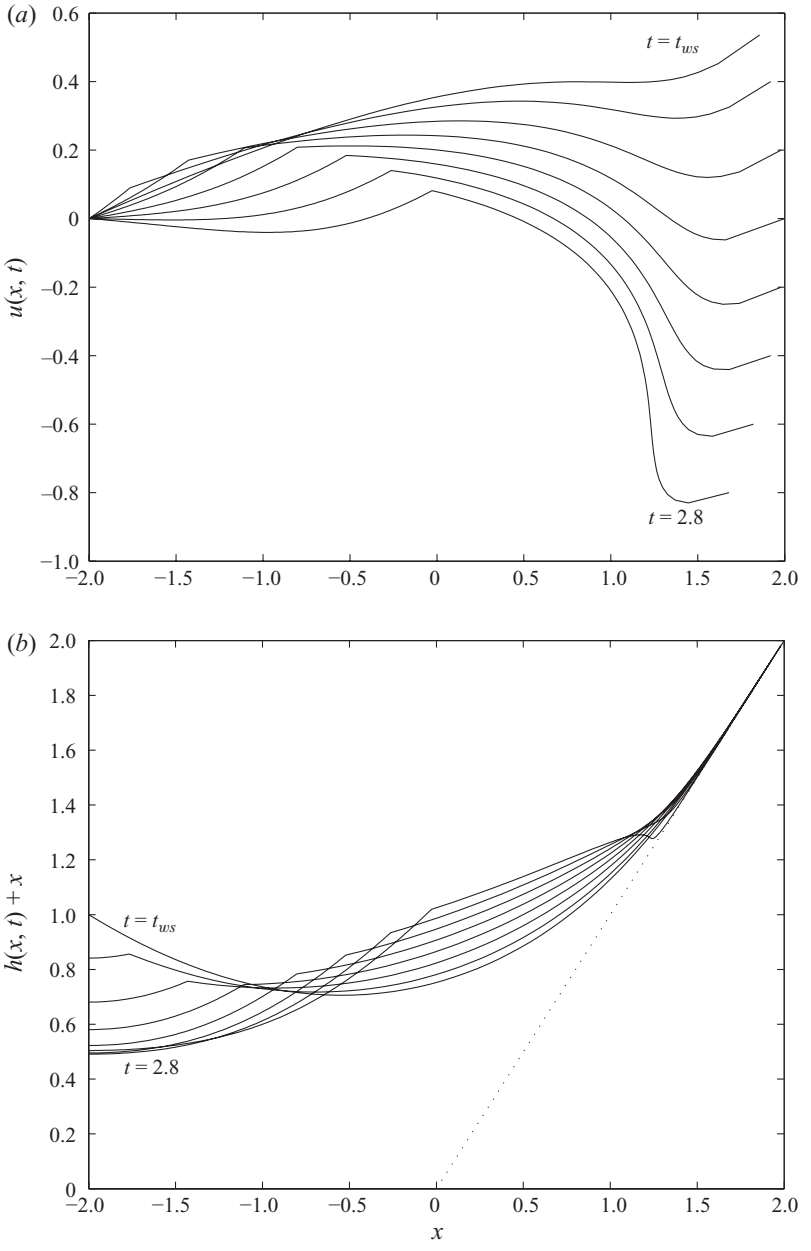

FIGURE 16. The velocity, $u(x, t)$, and elevation, $h(x, t) + x$, as functions of distance at various times after the rearmost β-characteristic has reached the back wall of the reservoir, in the case $L = 2$. The profiles are plotted at $t = t_{ws} (= 2\sqrt{3} - 2)$, 1.6, 1.8, 2.0, 2.2, 2.4, 2.6 and 2.8. The first and the last curve are labelled and during this interval the elevation of fluid at $x = -2$, $h(-2, t) - 2$, and the velocity, $u(1.5, t)$, progressively decrease. The fluid depth vanishes when the profile intersects the dotted line.

a fold at $\alpha = \alpha_{ws}$. The solution $t(\alpha_{ws}, \beta)$ is known, but subsequent evolution is in the direction of decreasing α; in other words, following a β-characteristic, we intersect $\alpha = \alpha_{ws}$ (the first α-characteristic that is affected by the back wall) and then subsequent propagation occurs for decreasing α. However, the range over which α decreases is

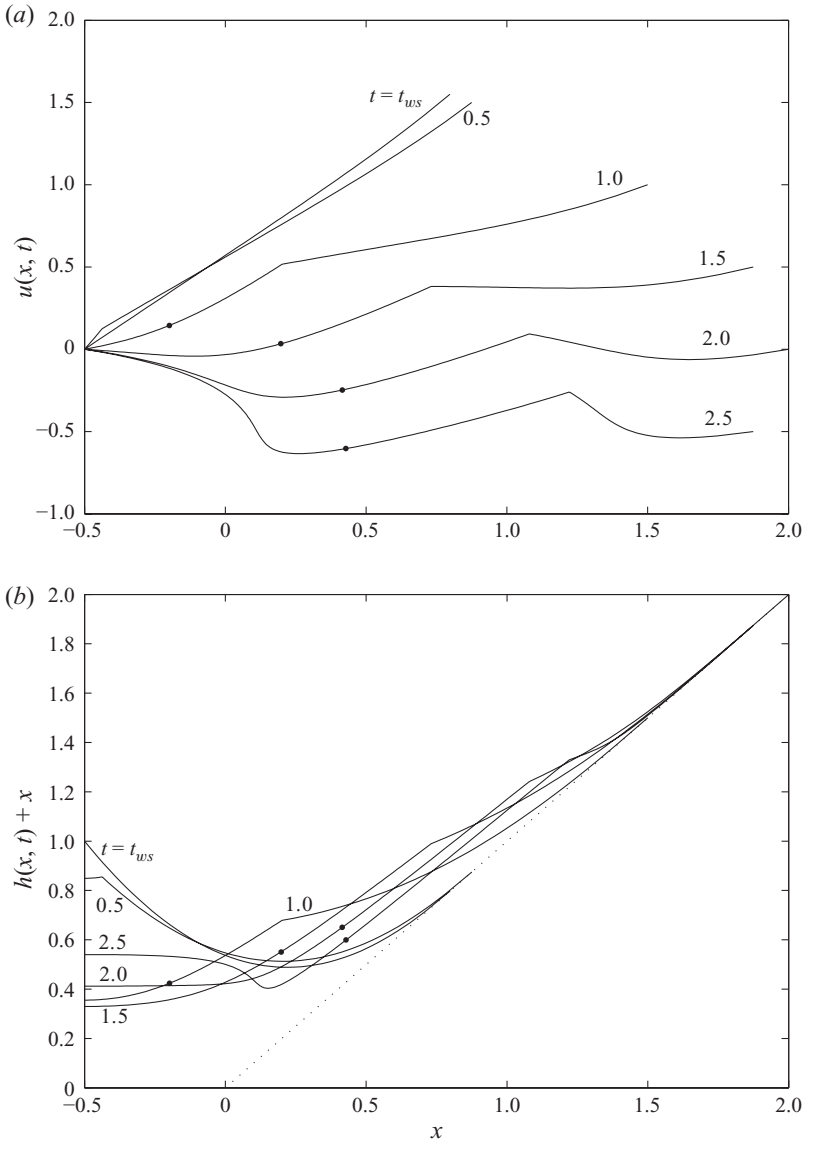

FIGURE 17. (*a*) The velocity, $u(x,t)$, and (*b*) elevation, $h(x,t)+x$, as functions of distance at various times after the rearmost β-characteristic has reached the back wall of the reservoir, in the case $L=0.5$. The profiles are plotted at $t=t_{ws}(=2\sqrt{3/2}-2)$, 0.5, 1.0, 1.5, 2.0 and 2.5, and the curves are labelled with the times. The position of the α-characteristic corresponding to $\alpha'_w=0$ is marked on the profiles for $1.0\leqslant t\leqslant 2.5$; it is noted that there is no change of gradient associated at these points. The fluid depth vanishes when the profile intersects the dotted line.

bounded by the value $\alpha=\alpha_b$ at which $\alpha'_w=0$. Thereafter, the hodograph plane develops another fold and subsequent propagation along β-characteristics occurs with increasing α. To construct the solution for $\alpha_b\leqslant\alpha\leqslant\alpha_{ws}$, we use (A 7) and this leads to the evaluation of $t(\alpha_b,\beta)$. Thereafter we use the contour EFG, where

$$E=(\alpha_b,\beta_b),\quad F=(\alpha_b,\beta)\quad\text{and}\quad G=(\alpha_w,\beta),\tag{A 9}$$

where $\alpha_w(\beta_b)=\alpha_b$. Parameterising the integration path using a and b as before and choosing $\alpha=\alpha_{ws}$, we find that

$$0=\left(\frac{\alpha_b-\beta}{\alpha_{ws}-\beta}\right)^{3/2}t(\alpha_b,\beta)-\left(\frac{\alpha_w-\beta}{\alpha_{ws}-\beta}\right)^{3/2}t(\alpha_w,\beta)+\int_{\beta_b}^{\beta}\left[\frac{-3B}{2(\alpha_b-b)}-\frac{\partial B}{\partial b}\right]t(\alpha_b,b)\,\mathrm{d}b$$
$$-\int_{\beta}^{\beta_b}\left[\frac{3tB}{2(a_w-b)}(a_w'+1)+t\frac{\partial B}{\partial b}+\frac{B}{4}(a_w'+1)\right]\mathrm{d}b. \quad (A\,10)$$

In the first integral of this expression, $B\equiv B(\alpha_b,b;\alpha_{ws},\beta)$ and likewise for its derivative, while in the second integral, $B\equiv B(a_w,b;\alpha_{ws},\beta)$ and likewise for its derivative. Then replacing $(\beta,\alpha_w(\beta),\hat{\beta})$ with (β_b,α_b,β) in (A 7) and summing with (A 10) establishes that (A 8) can be used to determine the curve in the hodograph plane that represents the condition of no flow at the back wall of the reservoir for all values of L, irrespective of whether the hodograph plane develops folds.

The equation for $t(\alpha_w,\beta)$ (i.e. (A 7)) is most readily solved numerically by differentiating with respect to β to generate the following Volterra equation, which may then be solved by successive iterations

$$\alpha_w'=4\left(\frac{\alpha_{ws}-\beta}{\alpha-\beta}\right)^{3/2}\frac{\partial t}{\partial\beta}-1+\frac{9}{2}\left(\frac{\alpha_w+\beta}{\alpha_{ws}-\beta}\right)\left(\frac{\alpha_{ws}-\alpha_w}{\alpha_w-\beta}\right)+\left(\frac{\alpha_{ws}-\beta}{\alpha-\beta}\right)^{3/2}$$
$$\times\int_{-2}^{\beta}\left[\frac{\partial B}{\partial\beta}(a_w'+1)\left(\frac{3(a_w+b)}{a_w-b}+1\right)+2(a_w+b)\frac{\partial^2 B}{\partial b\partial\beta}\right]\mathrm{d}b. \quad (A\,11)$$

In this expression, $\partial t/\partial\beta$ is evaluated at $(\alpha,\beta)=(\alpha_{ws},\beta)$. Typically, 10 iterations are required to obtain an accuracy of 10^{-6}. In figure 15, we plot the boundary curves in the hodograph plane for $L=2$ and $L=0.5$, the latter illustrating a situation in which the hodograph plane develops folds. Having computed this curve, it is straightforward to calculate times at other points in the hodograph plane by integrating around the contour $ABCD$. The positions, $x(\alpha,\beta)$, may be found by integrating along α-characteristics from the curve $\alpha=\alpha_w(\beta)$, using the condition that $x(\alpha_w,\beta)=0$. In figures 16 and 17, we plot profiles of the velocity, $u(x,t)$, and the elevation of fluid, $h(x,t)+x$, at various instances of time. We note that these profiles are continuous at the times plotted, though from Antuono & Hogg (2009), we anticipate that discontinuities may develop at later times as the fluid recedes. However, the profiles do exhibit discontinuities in their gradients, which occur at the position of the first forward-propagating α-characteristic ($\alpha=\alpha_{sw}$) and which arise due to the reflection of the rearmost β-characteristic at the wall ($x=-L$). We further note that the profiles for $L=0.5$, for which there are folds in the hodograph plane, do not exhibit any discontinuities when $\alpha_w'=0$; rather this is just a feature of the hodograph plane.

REFERENCES

Abramowitz, M. & Stegun, I. 1964 *A Handbook of Mathematical Functions*. AMS-55. National Bureau of Standards.

Antuono, M. & Hogg, A. J. 2009 Run-up and backwash bore formation from dam-break flow on an inclined plane. *J. Fluid Mech.* **640**, 151–164.

Antuono, M., Hogg, A. J. & Brocchini, M. 2009 The early stages of shallow flows in an inclined flume. *J. Fluid Mech.* **633**, 285–309.

Baldock, T. & Holmes, P. 1997 Swash hydrodynamics on a steep beach. In *Coastal Dynamics 97*, pp. 784–793. ASCE.

Baldock, T. E., Barnes, M. P., Morrison, N., Shimamoto, T., Gray, D. & Nielsen, O. 2007 Application and testing of the ANUGA tsunami model for overtopping and sediment transport. In *Coasts and Ports 2007, Melbourne, Australia.*

Baldock, T. E., Hughes, M. G., Day, K. & Louys, J. 2005 Swash overtopping and sediment overwash on a truncated beach. *Coast. Engng* **52**, 633–645.

Brocchini, M. & Dodd, N. 2008 Nonlinear shallow water equation modelling for coastal engineering. *J. Waterway, Port, Coast. Ocean Engng* **134**, 104–120.

Dodd, N. 1998 Numerical model of wave run-up, overtopping and regeneration. *J. Waterway, Port, Coast. Ocean Engng* **124** (2), 73–81.

Donnelly, C., Kraus, N. & Larson, M. 2006 State of knowledge on measurement and modeling of coastal overwash. *J. Coast. Res.* **22**, 965–991.

Garabedian, P. R. 1986 *Partial Differential Equations*. Chelsea Publishing.

Guard, P. A. & Baldock, T. E. 2007 The influence of seaward boundary conditions on swash zone hydrodynamics. *Coast. Engng* **54**, 321–331.

Henderson, F. M. 1966 *Open Channel Flow*. Macmillan.

Hine, A. C. 1979 Mechanics of berm development and resulting beach. *Sedimentology* **26**, 333–351.

Hogg, A. J. 2006 Lock-release gravity currents and dam-break flows. *J. Fluid Mech.* **569**, 61–87.

Hogg, A. J. & Pritchard, D. 2004*a* The effects of drag on dam-break and other shallow inertial flows. *J. Fluid Mech.* **501**, 179–212.

Hogg, A. J. & Pritchard, D. 2004*b* The transport of sediment over a sloping breakwater. In *Proceedings of the 15th Australasian Fluid Mechanics Conference* (ed. M. Behnia, W. Lin & G. D. McBain). Paper AFMC 00054. The University of Sydney, Australia.

Hu, K., Mingham, C. G. & Causon, D. M. 2000 Numerical simulation of wave overtopping of coastal structures using the non-linear shallow water equations. *Coast. Engng* **41**, 433–465.

Hubbard, M. E. & Dodd, N. 2002 A 2D numerical model of wave run-up and overtopping. *Coast. Engng* **47**, 1–26.

Hughes, M. G. 1995 Friction factors for wave uprush. *J. Coast. Res.* **11**, 1089–1098.

Kerswell, R. R. 2005 Dam break with Coulomb friction: a model for granular slumping? *Phys. Fluids* **17**, 057101(1–16).

Kobayashi, N., Tega, Y. & Hancock, M. W. 1996 Wave reflection and overwash of dunes. *J. Waterway, Port, Coast. Ocean Engng* **122**, 150–153.

Lauber, G. & Hager, W. H. 1998 Experiments to dambreak wave: horizontal channel. *J. Hydraul. Res.* **36**, 291–307.

Miller, R. L. 1968 Experimental determination of run-up of undular and fully developed bores. *J. Geophys. Res.* **73**, 4497–4510.

Peregrine, D. H. 1972 Equations for water waves and the approximations behind them. In *Waves on Beaches and Resulting Sediment Transport* (ed. R. Meyer), Chapter 3, pp. 95–121. Academic Press.

Peregrine, D. H. & Williams, S. M. 2001 Swash overtopping a truncated plane beach. *J. Fluid Mech.* **440**, 391–399.

Pritchard, D., Guard, P. A. & Baldock, T. E. 2008 An analytical model for bore-driven run-up. *J. Fluid Mech.* **610**, 183–193.

Pritchard, D. & Hogg, A. J. 2005 On the transport of suspended sediment by a swash event on a plane beach. *Coast. Engng* **52**, 1–23.

Puleo, J. A. & Holland, K. T. 2001 Estimating swash zone friction coefficients on a sandy beach. *Coast. Engng* **43**, 25–40.

Reis, M. T., Hu, K., Hedges, T. S. & Mase, H. 2008 A comparison of empirical, semiempirical and numerical wave overtopping models. *J. Coast. Res.* **24**, 250–262. doi:10.2112/05-0592.

Shen, M. C. & Meyer, R. E. 1963 Climb of a bore on a beach. Part 3: Run-up. *J. Fluid Mech.* **16**, 113–125.

Shiach, J. B., Mingham, C. G., Ingram, D. M. & Bruce, T. 2004 The applicability of the shallow water equations for modelling violent wave overtopping. *Coast. Engng* **51**, 1–15.

Synolakis, C. E. & Bernard, E. N. 2006 Tsunami science before and beyond Boxing Day 2004. *Phil. Trans. R. Soc.* A **364**, 2231–2265.

Weir, F. M., Hughes, M. G. & Baldock, T. E. 2006 Beach face and berm morphodynamics fronting a coastal lagoon. *Geomorphology* **82**, 331–346.

Whitham, G. B. 1955 The effects of hydraulic resistance in the dambreak problem. *Proc. R. Soc. Lond.* **227**, 399–407.